HHS Public Access

Author manuscript

Cell Metab. Author manuscript; available in PMC 2024 March 14.

Published in final edited form as:

Cell Metab. 2024 March 05; 36(3): 617–629.e7. doi:10.1016/j.cmet.2024.01.011.

DGAT2 inhibition blocks SREBP-1 cleavage and improves hepatic steatosis by increasing phosphatidylethanolamine in the ER

Shunxing Rong[1,2,5], **Mingfeng Xia**[1,4,5], **Goncalo Vale**[1,2], **Simeng Wang**[3], **Chai-Wan Kim**[1,2], **Shili Li**[1], **Jeffrey G. McDonald**[1,2], **Arun Radhakrishnan**[1], **Jay D. Horton**[1,2,3,6,*]

[1]Department of Molecular Genetics, University of Texas Southwestern Medical Center, Dallas, TX 75390-9046, USA

[2]Center for Human Nutrition, University of Texas Southwestern Medical Center, Dallas, TX 75390-9046, USA

[3]Department of Internal Medicine, University of Texas Southwestern Medical Center, Dallas, TX 75390-9046, USA

[4]Department of Endocrinology and Metabolism, Zhongshan Hospital, Fudan University, Shanghai 200032, China

[5]These authors contributed equally

[6]Lead contact

SUMMARY

Diacylglycerol acyltransferase 2 (DGAT2) catalyzes the final step of triglyceride (TG) synthesis. DGAT2 deletion in mice lowers liver TGs, and DGAT2 inhibitors are under investigation for the treatment of fatty liver disease. Here, we show that DGAT2 inhibition also suppressed SREBP-1 cleavage, reduced fatty acid synthesis, and lowered TG accumulation and secretion from liver. DGAT2 inhibition increased phosphatidylethanolamine (PE) levels in the endoplasmic reticulum (ER) and inhibited SREBP-1 cleavage, while DGAT2 overexpression lowered ER PE concentrations and increased SREBP-1 cleavage *in vivo*. ER enrichment with PE blocked SREBP-1 cleavage independent of Insigs, which are ER proteins that normally retain SREBPs in the ER. Thus, inhibition of DGAT2 shunted diacylglycerol into phospholipid synthesis, increasing the PE content of the ER, resulting in reduced SREBP-1 cleavage and less hepatic steatosis.

*Correspondence: jay.horton@utsouthwestern.edu.

AUTHOR CONTRIBUTIONS

S.R., M.X., G.V., S.L., S.W., C.-W.K., and J.G.M. conducted experiments. A.R. provided reagents and advice for ER isolation and measurement of accessible cholesterol levels in ER. J.D.H., S.R., and M.X. designed the research. S.R., M.X., S.W., and J.D.H. wrote the manuscript.

SUPPLEMENTAL INFORMATION

Supplemental information can be found online at https://doi.org/10.1016/j.cmet.2024.01.011.

DECLARATION OF INTERESTS

J.D.H. is on the scientific advisory board for Merck and Pfizer and a consultant for Regeneron.

This study reveals a new mechanism that regulates SREBP-1 activation and lipogenesis that is independent of sterols and SREBP-2 in liver.

Graphical abstract

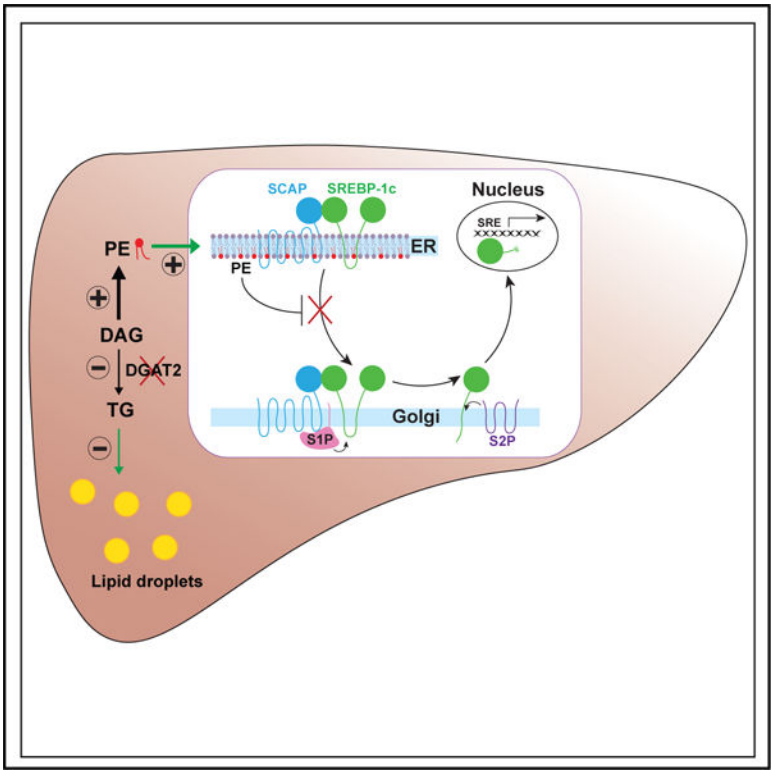

In brief

DGAT2 inhibition blocks triglyceride synthesis in liver and is a promising new approach for the treatment of steatotic liver diseases. Rong et al. show that DGAT2 inhibition has a dual effect: it not only blocks the last step of triglyceride synthesis but also suppresses SREBP-1, the transcriptional activator of lipogenesis in liver.

INTRODUCTION

Nonalcoholic fatty liver disease (NAFLD), which has been recently renamed metabolic dysfunction-associated steatotic liver disease (MASLD),[1] is characterized by the accumulation of triglycerides (TGs) in hepatocytes and is the leading cause of chronic liver disease and hepatocellular carcinoma in the US.[2–5] It is estimated that a quarter of the global population is currently affected by MASLD.[5] Excess TG accumulation in livers of individuals with MASLD can lead to nonalcoholic hepatitis (NASH) (now renamed metabolic dysfunction-associated steatohepatitis [MASH]), cirrhosis, and hepatocellular carcinoma.[6,7] Reducing liver TG accumulation is currently one strategy under investigation for treating individuals with MASLD.[8]

One underlying metabolic alteration that contributes to TG accumulation in the livers of individuals with MASLD is increased *de novo* lipogenesis.[3,9] Pharmacological inhibitors of enzymes in the fatty acid synthesis pathway, such as ATP-citrate lyase (ACL), acetyl-CoA carboxylase (ACC), and fatty acid synthase (FAS), are in early-stage clinical trials.[10–13] One inhibitor of TG synthesis, diacylglycerol acyltransferases 2 (DGAT2), is also in clinical trials.[14,15] DGATs carry out the final step of TG synthesis by catalyzing the addition of acyl-CoAs to diacylglycerol (DAG), forming TGs.[16]

Two structurally unrelated DGAT enzymes, DGAT1 and DGAT2, have been identified.[17–19] DGAT1 preferentially utilizes exogenous fatty acids for TG synthesis,[20] while DGAT2, which is abundantly expressed in liver, predominantly synthesizes TGs using fatty acids derived from *de novo* lipogenesis.[21] DGAT2 expression has previously been shown to be important for the development of hepatic steatosis.[22–26] Results from recent clinical trials reported that administration of a DGAT2 inhibitor alone or in combination with an ACC inhibitor to individuals with MASLD significantly improved hepatic steatosis and liver function tests.[14,15]

The mechanism by which DGAT2 inhibition improves liver steatosis has not been fully elucidated. In addition to blocking the last step in TG synthesis, SREBP-1c-regulated genes responsible for fatty acid synthesis were also decreased when DGAT2 was deleted or inhibited in animals.[14,22–26] It is not clear how or why DGAT2 blockade selectively suppresses SREBP-1c and *de novo* fatty acid synthesis.

SREBPs are membrane-bound transcription factors located in the endoplasmic reticulum (ER) as inactive precursors where they form a complex with SCAP, a cholesterol sensor. When cellular cholesterol levels exceed a threshold concentration, the SCAP/SREBP complex binds to Insigs, which retain the SCAP/SREBP complex in the ER.[27] When cellular cholesterol levels drop below the threshold concentration, the SCAP/SREBP complex is released from Insigs and moves from the ER to Golgi, where SREBPs are cleaved sequentially by the proteases S1P and S2P, which release the transcriptionally active form of SREBPs. There are three isoforms of SREBPs in mammalian cells: SREBP-1a, SREBP-1c, and SREBP-2.[28] SREBP-2 primarily regulates the expression of enzymes for cholesterol synthesis, while SREBP-1c is the major SREBP-1 isoform in liver that regulates the expression of genes encoding enzymes for fatty acid and TG syntheses.[28,29] To date, the available studies suggest that all SREBP isoforms use the same Insig/SCAP machinery for sterol-mediated regulation of cleavage.[28,30,31]

Here, we use a DGAT2 inhibitor, liver-specific DGAT2 knockout mice, and DGAT2 overexpression in mice to further characterize the molecular mechanism by which DGAT2 inhibition reduces *de novo* lipogenesis and improves hepatic steatosis. We found that DGAT2 deletion in hepatocytes or pharmacologic DGAT2 inhibition increased the phosphatidylethanolamine (PE) content of the ER, and this prevented SREBP-1 cleavage, which reduced hepatic *de novo* lipogenesis and reduced TG accumulation and secretion from liver. Enrichment of PE in the ER by supplementation of high-PE-containing liposomes or ethanolamine blocked SREBP-1 cleavage in cultured cells. Using DGAT2 inhibition as a tool, we have uncovered a new mechanism that independently regulates the

activation of SREBP-1 and *de novo* lipogenesis in a manner that is independent of Insigs in mammalian cells.

RESULTS

Inhibition of DGAT2 reduced plasma and liver lipid levels by suppressing SREBP-1c and hepatic *de novo* lipogenesis

In mice and human clinical studies, DGAT2 inhibition reduced hepatic steatosis.[14,15,22–24,26] To determine the mechanism by which the inhibition of DGAT2 decreases liver TG content, a DGAT2 inhibitor (iDgat2, Sigma Cat# PZ0233) was fed to C57BL/6J mice for 7 days (0.004% mixed in chow). The dose of the DGAT2 inhibitor chosen was based on the dose and pharmacokinetics parameters published previously.[14,32] The phenotypic parameters of the mice treated with iDgat2 are summarized in Table 1. Administration of iDgat2 did not change food intake, body weights, liver weights, blood glucose, or insulin levels. As shown previously, C57BL/6J mice treated with iDgat2 had dramatically lower liver TG concentrations.[14,15,22–26] Liver cholesterol content was not affected by iDgat2 treatment. Plasma cholesterol and TG levels were also significantly reduced with iDgat2 treatment.

To determine whether SREBP-regulated *de novo* lipogenesis was affected by iDgat2 administration, RNA and protein were prepared from livers, and SREBP-regulated genes and proteins were evaluated by quantitative real-time PCR and immunoblot analysis, respectively. SREBP-1c mRNA levels were lowered ~50% in livers of iDgat2-treated mice. Accordingly, SREBP-1c-regulated genes, including acetyl-CoA synthetase-2 (ACSS-2), ACL, ACC-1, ACC-2, FAS, and PNPLA3, were all significantly reduced in livers of iDgat2-treated mice (Figure 1A). Consistent with the measured mRNA levels, protein levels of the precursor membrane-bound form of SREBP-1 (P) and the active nuclear form (N) of SREBP-1 were decreased in response to DGAT2 inhibition (Figures 1B and 1C). Gene expression of SREBP-2 and other sterol-synthesis genes including HMG-CoA synthase (HMG S), HMG-CoA reductase (HMG R), and squalene synthase (SS) were similar in control and iDgat2-treated mouse livers (Figure S1). Neither the precursor (P) nor the (N) form of SREBP-2 was affected by DGAT2 inhibition (Figures 1B and 1C). The expression of PCSK9 was slightly reduced after iDgat2 treatment (Figure S1), which could contribute to the lower plasma cholesterol levels observed. Activation of the nuclear receptor, LXR, is required for the expression of SREBP-1c and lipogenic genes.[33,34] The expression of Cyp7a1 and ChREBP, target genes of LXR not regulated by SREBP-1, was not changed by DGAT2 inhibition (Figure S1), indicating that the suppression of SREBP-1 and lipogenesis is independent of LXR activity.

As shown in Table 1, plasma TG and cholesterol levels were significantly reduced by iDgat2 administration. To investigate whether the reduced plasma lipid levels were a result of decreased lipid secretion from liver, VLDL secretion was measured in mice treated with iDgat2 for 7 days. As shown in Figures 1D and 1E, TG secretion rates were significantly decreased with iDgat2 administration following triton injection.

To confirm that DGAT2 inhibition improves MASLD in mice, *ob/ob* mice were fed either chow or the chow diet containing the DGAT2 inhibitor for 7 days. DGAT2 inhibition

did not change body weights, plasma insulin, or glucose levels of *ob/ob* mice (Figures S2A, S2E, and S2F); however, liver weights and liver TGs were significantly reduced by 11% and 51%, respectively (Figures S2B and S2C). Liver cholesterol was not affected by iDgat2 treatment (Figure S2D). Similar to the results from C57BL/6J iDgat2-treated mice, SREBP-1c-regulated gene expressions of ACSS-2, ACL, ACC-1, ACC-2, FAS, and PNPLA3 were all significantly decreased by 34%–61% in livers of iDgat2-treated mice (Figure S2G). Immunoblot analysis again showed a marked reduction in nSREBP-1 protein levels in livers of iDgat2-treated mice (Figures S2I and S2J). Combined, the results from C57BL/6J and *ob/ob* mice indicate that iDgat2 inhibits SREBP-1c and reduces SREBP-1c-regulated *de novo* lipogenesis.

Inhibition of DGAT2 blocks the activation of SREBP-1

Cleaved nSREBP-1 was dramatically reduced in both wild-type and *ob/ob* mice when DGAT2 was inhibited (Figures 1B, 1C, S2I, and S2J). A recent study using a RNAi to knock down DGAT2 expression in livers of mice showed that nSREBP-1 was reduced by DGAT2 depletion without affecting the precursor SREBP-1.[26] However, mRNA and precursor SREBP-1c protein levels in wild-type mice of our current study were decreased, possibly due to greater DGAT2 inhibition. Inasmuch as there is a positive feedback loop in which SREBP-1c transcriptionally activates its own promoter,[35] the decrease of SREBP-1 expression could be a result of either reduced transcription or inhibition of SREBP cleavage.

To determine if DGAT2 inhibition directly altered SREBP-1 cleavage, we took advantage of a previously generated transgenic rat that constitutively expresses HA-tagged human full-length (precursor) SREBP-1c under the control of the apoE promoter (TghSREBP-1c).[36] TghSREBP-1c rats were fed chow or chow supplemented with iDgat2 for 7 days. The TghSREBP-1c rats showed the same metabolic phenotype as the C57BL/6J mice after iDgat2 administration (Table 1). Food consumption, body weights, liver weights, blood glucose and plasma insulin levels, and liver cholesterol concentrations were not changed by DGAT2 inhibition. Plasma cholesterol and TGs levels and liver TGs in the transgenic rats were decreased significantly after 7 days of iDgat2 administration.

As was found in wild-type mice, endogenous rat SREBP-1c (rSREBP-1c) mRNA levels were significantly reduced in livers following DGAT2 inhibition, but the transgenic human SREBP-1c (hSREBP-1c) mRNA levels were not affected (Figure 2A). Immunoblot analysis using an SREBP-1 antibody that recognizes both endogenous rat SREBP-1 and transgenically expressed human SREBP-1 protein revealed a significant reduction in nSREBP-1 with iDgat2 inhibition (Figures 2B and 2C). Importantly, immunoblot analysis of only transgenically expressed human SREBP-1 using an anti-HA antibody showed that only the nuclear form but not the precursor form of SREBP-1 was reduced by iDgat2 treatment (Figures 2B and 2C). As expected, reduced nSREBP-1 was associated with the reduction of ACSS-2, ACL, ACC-1, ACC-2, FAS, and PNPLA3 mRNA levels (Figure 2A). Combined, these results suggest that DGAT2 inhibition leads to a reduction in SREBP-1 cleavage, and this in turn leads to decreased lipogenesis.

Cholesterol content in the ER is not altered by iDgat2

Detailed studies in cultured cells have provided insights into how cholesterol regulates the activation of SREBPs.[37–45] These studies have shown that only a small portion of total cellular cholesterol resides in the ER membrane where it can bind SCAP, which permits the SCAP/SREBP complex to bind Insigs, preventing the transport of the SCAP/SREBP complex from the ER to Golgi.[46]

To further investigate the mechanism by which DGAT2 inhibition blocked SREBP-1 activation, we first measured the sterol content in the ER of TghSREBP-1c rats treated with or without iDgat2 for 7 days. ER fractions were isolated from the rat livers,[41] and the purity of the ER isolated was confirmed by immunoblot analysis using organelle-specific protein markers (Figure S3). Cholesterol levels in the ER fractions were measured using mass spectrometry. Cholesterol levels in the ER fractions were not affected by the inhibition of DGAT2 when either normalized to total ER protein content or expressed as molar percentage of total ER lipids (Figures S4A and S4B). Concentrations of other sterols and oxysterols in the ER fractions were also similar in control and iDgat2-treated groups (Figure S4C).

Inasmuch as the total levels of ER cholesterol were unchanged, we next determined whether the distribution of cholesterol into sequestered and accessible pools[46] was affected by iDgat2 treatment. To investigate, we used ALOD4, a sensor that specifically binds to the small portion of ER cholesterol, termed accessible cholesterol, that regulates SREBP activation.[40,47,48] ALOD4 binding to purified ER membrane fractions from chow and iDgat2-treated transgenic rats was measured, and no difference in the binding of ALOD4 was observed (Figure S4D). Combined, these results suggest that DGAT2 inhibition does not change the total ER cholesterol content or the levels of accessible cholesterol in the ER and that the observed reduction in SREBP-1 cleavage is not cholesterol mediated.

Inhibition of DGAT2 increases PE content in ER

To uncover the nature of the cholesterol-independent reduction of SREBP-1 cleavage by iDgat2, we examined in greater detail the metabolic fate of DAGs. In addition to being a precursor for TG synthesis, DAG is also an intermediate for phospholipid synthesis. Blocking DGAT2, therefore, could also redirect DAGs into the phospholipid synthesis pathway and change the phospholipid content of the ER. To test this possibility, the phospholipid content in ER fractions of livers from control and iDgat2-treated TghSREBP-1c rats were quantified by liquid chromatography with tandem mass spectrometry (LC-MS/MS). The only consistent change measured was a significant increase in the PE content in the ER (Figure 3A). Other major ER lipids such as DAG, phosphatidylcholine (PC), phosphatidylglycerol (PG), phosphotidylinositol (PI), and phosphatidylserine (PS) were similar in control and iDgat2 groups. The fatty acid composition of the major ER phospholipid species (PC and PE) was also not affected by the inhibition of DGAT2 (Figures 3D and 3E).

To confirm that the PE concentrations were increased in ER following iDgat2 administration, ER fractions of livers from C57BL/6J and *ob/ob* mice that were administered

iDgat2 for 7 days were prepared and subjected to lipidomic measurements using LC-MS/MS. Consistent with the results from TghSREBP-1c rats, DGAT2 inhibition led to a significant increase in the PE content of the ER in both C57BL/6J and *ob/ob* mice (Figures 3B and 3C). In C57BL/6J mice treated with iDgat2, DAG levels were also statistically increased. Other ER phospholipids including PC, PI, PS, and PG were not changed by DGAT2 inhibition (Figure 3B). In *ob/ob* mice, all phospholipid species increased, which is consistent with the results from a recent study from Yenilmez et al.[26]; however, the increase in PE was greater than that of the two other major ER phospholipids PC and PI (Figure 3C). Thus, in all the three animal models, DGAT2 inhibition consistently increased PE levels in the liver ER fractions.

To investigate whether ER stress was affected by the change of PE levels in the ER, the mRNA levels of XBP1 (XBP1u, unspliced form, and XBP1s, spliced form), Ddit3, and Atf4 were measured in C57BL/6J (Figure S1B) and *ob/ob* mice (Figure S2H) treated with iDgat2. As shown in Figures S1B and S2H, DGAT2 inhibition did not change the ER stress related gene expression.

To confirm that the increase in the ER content of PE caused by iDgat2 was not due to an off-target effect of the drug, we deleted *Dgat2* in hepatocytes using an adeno-associated virus (AAV)-DJ-expressed sgRNA in Cas9-expressing mice. Consistent with our findings using the DGAT2 inhibitor, the genetic deletion of *Dgat2* also resulted in increased PE levels in the ER, which was associated with a dramatic reduction of nSREBP-1 (Figures 6C–6E).

Inasmuch as DGAT2 inhibition resulted in increased ER PE content, we hypothesized that elevated DGAT2 activity might have the opposite effect. To test this hypothesis, mouse DGAT2 was overexpressed in C57BL/6J mice using AAV8 (scAAV8.CB6-mDgat2). The tissue specificity of AAV8 and AAV-DJ was first evaluated. mCherry-expressing AAV8 or AAV-DJ was injected into C57BL/6J mice. Immunoblot analysis showed that in both AAV8-mCherry- and AAV-DJ-mCherry-injected mice, mCherry protein was only detectable in liver and not in other tissues such as adipose tissue, muscle, heart, etc. (Figure S7A). To confirm that AAV8 and AAV-DJ only infected hepatocytes and not the other cells in the liver, we carried out single-cell sequencing of liver cells isolated from mice infected with AAV8-mCherry and AAV-DJ-GFP. The mCherry and GFP signals were highly expressed in albumin- and apoB-expressing hepatocytes and not in stellate, endothelial, or Kupffer cells (Figure S7B).

Next, scAAV8.CB6-mDgat2-injected mice were fed a fat-free diet for 1 week to stimulate lipogenesis and DAG production before samples were collected for analysis. Overexpression of DGAT2 was confirmed by quantitative real-time PCR (Figure S5E). Body weights, liver weights, and liver cholesterol levels were not affected by the overexpression of DGAT2; however, liver TG concentrations were significantly increased by DGAT2 overexpression (Figures S5A–S5D). The increased liver TG levels were accompanied by increased nSREBP-1c protein and elevated SREBP-1c, ACL, ACC-1, and PNPLA3 mRNA levels (Figures S5E–S5G). Importantly, the PE content of ER from livers overexpressing DGAT2 was reduced, while the PC levels maintained a similar level as the control mice (Figure S5F).

Inasmuch as nSREBP-1 is chronically elevated in livers of *ob/ob* mice,[49] the relationship of SREBP-1 cleavage and PE content in the ER was measured and compared with that in C57BL/6J mice. Cleaved nSREBP-1 was increased dramatically in livers from *ob/ob* mice, consistent with previous reports[49] (Figures S6A and S6B). The measured PE levels in the liver ER fractions prepared from *ob/ob* mice were reduced 75% compared with those in controls (Figure S6C). In contrast, ER PC levels were similar between C57BL/6J and *ob/ob* mice (Figure S6C). These results suggest that the ER content of PE plays a crucial role in the physiological regulation of SREBP-1 activation.

PE enrichment suppresses SREBP-1 cleavage

Insect cells do not synthesize sterols and have only one isoform of SREBP that regulates the genes involved in fatty acid biosynthesis.[50] Instead of cholesterol, PE is the lipid in the ER of *Drosophila* cells that regulates the activation of SREBP.[51] To investigate whether the PE in ER could directly regulate SREBP-1 activation in mammalian cells, liposomes with different PE concentrations were introduced into the ER of primary hepatocytes isolated from TghSREBP-1c rats.[52,53] The incubation of cells with low-PE- or high-PE-containing liposomes only changed the PE levels in the ER membranes and not in whole-cell membranes (Figure 4A). To determine whether increased PE content in the ER blocked SREBP-1 activation, membrane and nuclear proteins were prepared from TghSREBP-1c rat primary hepatocytes and subjected to immunoblot analysis using the anti-HA tag antibody that recognizes the transgenically expressed human SREBP-1c. As shown in Figure 4B, nSREBP-1c was significantly reduced in cells supplemented with high-PE-containing liposomes. Conversely, nSREBP-1 was increased in cells supplemented with low-PE-containing liposomes (Figure 4B). Similar results were obtained using the mouse hepatoma cell line, Hepa-1c1c7 (Figure 4C). These results suggest that DGAT2 inhibition shunts DAG to PE, which accumulates in the ER and blocks SREBP-1 processing.

We next confirmed that the effect of PE was specific for SREBP-1 cleavage and not SREBP-2. Free ethanolamine serves as the precursor for PE synthesis by base exchange with PS. Ethanolamine can also be converted directly to PE and serves as the intermediate for PE synthesis.[54] Human fibroblast SV589 cells were enriched with PE by supplementing the medium with 0, 10, 20, and 50 μM of free ethanolamine for 18 h prior to harvesting the cells for immunoblot analysis. As shown in Figure 5A, nSREBP-1 was reduced by 43%–56% with ethanolamine supplementation, while nSREBP-2 was not significantly changed.

Insigs are not required for the suppression of SREBP-1 cleavage by PE

Insigs are not expressed in insect cells, indicating that the regulation of SREBP by PE in *Drosophila* cells is Insig independent.[51] To determine whether the regulation of SREBP-1 activation by PE in mammalian cells requires Insigs, we knocked out Insig-1 and Insig-2 in the human fibroblast cells (SV589) using CRISPR-Cas9 technology. Deletion of Insigs was confirmed by immunoblot analysis using an antibody that recognizes both Insig-1 and Insig-2 proteins[55] (Figure 5B). In *Drosophila*, palmitate can serve as a precursor for sphingosine-1-phosphate synthesis, and the synthesized sphingosine-1-phosphate can donate the phosphate group to ethanolamine to form phosphoethanolamine, which is eventually converted to PE.[51]

To determine if the PE regulation of SREBP-1 cleavage required Insigs in mammalian cells, control SV589 cells or Insig-deficient SV589 cells were enriched with PE by the supplementation of palmitate and/or ethanolamine. SREBP-1 activation was evaluated by immunoblot analysis. Deletion of Insigs significantly increased nSREBP-1 protein levels (Figure 5B, lanes 1–4 vs. lanes 5–8). Compared with the vehicle control, supplementation of palmitate alone did not significantly reduce nSREBP-1 protein levels (Figure 5B, lane 1 vs. 2 and lane 5 vs. 6). However, ethanolamine alone or in combination with palmitate significantly reduced nSREBP-1 protein in both control cells and Insig knockout cells (Figure 5, lanes 3 and 4 vs. lane 1, and lanes 7 and 8 vs. lane 5), demonstrating that PE-mediated suppression of SREBP-1 cleavage is Insig independent.

To confirm that SREBP-1 activation by DGAT2 inhibition was Insig independent *in vivo*, Insigs and/or DGAT2 knockout mice were generated by the injection of AAV-DJ-containing sgRNAs that target liver Insigs and/or DGAT2 into Cas9-expressing mice. Successful gene disruption was confirmed by quantitative real-time PCR (Figure 6A). Total mRNA levels of DGAT2 and Insig-1 were reduced by ~90%, while Insig-2a and Insig-2b mRNA levels were reduced by more than 60% (Figure 6A). The deletion of Insigs was further confirmed by immunoblot analysis, which showed undetectable protein levels using an Insig antibody that recognizes both Insig-1 and Insig-2 (Figure 6C). The mRNA levels of SREBP-1c-regulated genes (ACSS-2, ACL, ACC-1, ACC-2, FAS, and PNPLA3) were all significantly reduced in livers of DGAT2-deleted mice, in both control and Insig knockout backgrounds (Figure 6B).

Body weights and liver cholesterol levels were not affected by the deletion of DGAT2 in both control and Insig knockout backgrounds (Figure S7C). Liver weights were reduced in DGAT2;Insig knockout mice. Plasma cholesterol and TG levels and liver TG concentrations were significantly reduced when DGAT2 was deleted in both control and Insig knockout backgrounds (Figure S7C). PE levels in the ER fractions were significantly increased by DGAT2 deletion, in both control and Insig knockout backgrounds with no significant change in PC levels (Figure 6E). Consistently, nSREBP-1 protein was reduced significantly in livers of DGAT2 liver-specific knockout mice (Figures 6C and 6D). Hepatocyte deletion of Insig-1 and Insig-2 increased both precursor and nuclear forms of SREBP-1 protein in liver due to the unrestrained movement of the SCAP/SREBP complex to the Golgi for cleavage.[56,57] Importantly, nSREBP-1 was decreased in mice lacking both Insigs and DGAT2, confirming that the suppression of SREBP-1 cleavage is independent of Insigs *in vivo* (Figures 6C and 6D).

To further confirm that the decrease in nSREBP-1 in DGAT2 knockout livers was a result of reduced translocation of precursor SREBP-1 from the ER to the Golgi, we carried out an ER vesicle budding assay using microsomes prepared from livers of control, DGAT2 knockout, Insig knockout, and DGAT2;Insig knockout mice. Deletion of DGAT2 dramatically reduced the budding of SREBP-1, but not SREBP-2 (Figure S7D, lane 6 vs. lane 5, and lane 8 vs. lane 7), in both control and Insig knockout backgrounds. This suggests that the high PE content in the liver prevents the incorporation of the precursor SREBP-1 into CopII-coated vesicles that transport SREBP-1 to the Golgi for cleavage.

DISCUSSION

In this study, we have clarified the molecular mechanism by which DGAT2 inhibition blocks SREBP-1 cleavage, reduces FA and TG synthesis, and ultimately improves hepatic steatosis. DGAT2 inhibition increased the ER content of PE, which blocked SREBP-1 movement from the ER to Golgi for cleavage. We confirmed that the PE concentration of the ER regulated SREBP-1 activation *in vitro* by altering the relative concentrations of PE and showed that the high levels of PE in the ER reduced SREBP-1 activation. Conversely, low PE levels in the ER led to increased SREBP-1 cleavage. This was confirmed *in vivo* by overexpressing DGAT2 in liver, which reduced ER PE concentrations and increased SREBP-1 cleavage. Similarly, in insulin-resistant *ob/ob* mice, in which nSREBP-1 levels in liver are chronically high, we found that the PE concentrations in the liver ER were low, suggesting that the ability of PE to regulate SREBP-1 processing was not unique to DGAT2 inhibition. Finally, we showed that the ability of the ER PE concentrations to regulate SREBP-1 activation was independent of Insigs *in vitro* and *in vivo*, which also renders it independent of cholesterol-medicated SREBP regulation.

Animal studies and recent human clinical trials have shown that DGAT2 inhibition improves hepatic steatosis and represents a promising new target for the treatment of MASLD.[14,15,22,23] DGAT2 catalyzes the final step of TG synthesis in liver by adding *de-novo*-synthesized fatty acyl-CoAs to DAGs.[16,17,20,21] The direct effect of the DGAT2 inhibitor (PF-06424439) on TG synthesis and its ability to reduce SREBP-1-regulated lipogenic gene expression was shown by Futatsugi et al.[32] Here, we investigated the underlying molecular mechanism for this observation initially by treating animal models C57BL/6J and *ob/ob* mice and TghSREBP-1c rats with a DGAT2 inhibitor. In all models, inhibition of DGAT2 blocked the activation of liver SREBP-1, which reduced liver fatty acid synthesis and liver TGs (Figures 1B, 1C, 2B, 2C, S2I, and S2J). Inhibition of DGAT2 in *ob/ob* mice led to reduced nSREBP-1c protein with no changes in the mRNA or SREBP-1 precursor (Figures S2), which suggested that there was a specific effect on SREBP-1 cleavage that was independent of transcription.

Yenilmez et al.[26] previously reported that DGAT2 suppression using siRNA reduced nSREBP-1 levels; whether this was specifically due to the inhibition of SREBP cleavage could not be assessed.[35] To determine if DGAT2 inhibition blocked SREBP-1 cleavage, we took advantage of TghSREBP-1c rats that expressed human SREBP-1c under the control of a constitutive apolipoprotein E promoter/enhancer.[36] In TghSREBP-1c rats that were fed chow supplemented with iDgat2, the nhSREBP-1 (detected by anti-HA antibody) was significantly reduced, while the precursor hSREBP-1 protein and hSREBP-1c mRNA levels were not changed (Figure 2). The specific effect of DGAT inhibition on SREBP-1 and not SREBP-2 cleavage was further confirmed using the vesicle budding assays (Figure S7D).

Inasmuch as the suppression of SREBP-1 by DGAT2 inhibition resulted from the inhibition of SREBP-1 cleavage, we further investigated the potential underlying mechanism first by examining the lipid composition of the ER. The Brown and Goldstein laboratory has previously shown that the interaction of the SCAP:SREBP complex with Insig is enhanced with increasing cholesterol levels in the ER.[41,58] However, we found that the

cholesterol levels in the ER were unchanged as was the amount of accessible cholesterol following DGAT2 inhibition, which suggested that the classical modality of cholesterol-mediated SREBP suppression was not responsible for the SREBP-1 suppression. This is also consistent with the finding that suppression of SREBP-1 cleavage was not dependent on the interaction of SCAP:SREBP-1 with the retention proteins Insig-1 and/or Insig-2 *in vitro* or *in vivo* (Figures 5 and 6).

The only significant change in ER lipid composition that we consistently found associated with the changes in SREBP-1 cleavage was PE (Figure 3). In the iDgat2-treated animals, decreased SREBP-1 processing coincided with increased PE content in ER. Further *in vitro* studies with multiple cell lines showed that the activation of SREBP-1 was blocked when PE or substrates of PE synthesis were supplemented (Figures 4 and 5). Dobrosotskaya et al.[51] previously showed that high levels of PE synthesis in *Drosophila* leads to the suppression of SREBP cleavage. Insect cells do not have the enzymes necessary to synthesize cholesterol,[50] and the *Drosophila* genome only contains one homolog of SREBP, which is most closely related to the SREBP-1 isoform in mammalian cells and is responsible for the regulation of genes required for fatty acid synthesis.[50,59] The *Drosophila* genome also does not contain *Insig-1* or *Insig-2*, but it does have *Scap*. Here, the deletion of Insig-1 and −2 in human-cultured fibroblasts or in livers of mice did not affect the regulation of SREBP-1 processing by PE (Figures 5 and 6). Combined, the current studies indicate that the PE content in the ER of mammalian cells plays a similar role as that of *Drosophila* cells to regulate SREBP-1 activation and that this mechanism is evolutionarily conserved.

Recently, Rong et al.[53] reported that LXR induced the expression of LPCAT3, which preferentially catalyzes the synthesis of PC with polyunsaturated fatty acyl chains.[53] The relatively high content of linoleoyl and arachidonoyl PC in the ER membrane stimulated SREBP-1c activation. However, DGAT2 inhibition did not change the fatty acid compositions of either PC or PE (Figures 4C and 4D), which suggests that ER PE concentrations can regulate SREBP-1 activity using a mechanism that is distinct from that of LPCAT3-induced changes of fatty acyl chain composition.

How does inhibition of DGAT2 result in increased PE in the ER? TGs, PC, and PE share DAGs as substrates for their final biosynthesis steps. When TG synthesis is blocked by DGAT2 inhibition, DAGs can be directed into the PC or PE synthesis pathways. Since PC accounts for ~60% of the phospholipids in the ER,[60] the increased availability of DAG as substrate for synthesis might not significantly alter the PC content of the ER. However, considering the relatively low PE content in the ER membrane, even a slight increase of PE synthesis could result in a significant increase in the PE concentration.

The current studies provide evidence for a new mechanism of regulating SREBP-1 cleavage in mammals that is distinct from cholesterol-mediated SREBP regulation. We and others have published previously that SREBP-1 and SREBP-2 can be independently regulated in livers of mice in a manner that could not be recapitulated *in vitro*.[10,36,61,62] Examples of SREBP-1- and SREBP-2-independent regulation include the following: responses to high insulin levels such as in a refed or insulin-resistant animal where nSREBP-1 levels are much greater than nSREBP-2;[49,63,64] cholesterol feeding, where nSREBP-2 levels are suppressed

but nSREBP-1 levels are not[33]; and in response to polyunsaturated fatty acids, which suppress SREBP-1 but not SREBP-2.[10,36,61,62] Inasmuch as SREBP-1 and SREBP-2 both use the same basic regulatory machinery, it was assumed that discordant nSREBP levels were largely a result of differences in transcriptional activation. Our studies provide clear evidence that there is independent regulation of SREBP-1 cleavage that is mediated by the changes in the content of PE in the ER.

Recent clinical trials have shown that the inhibition of DGAT2 significantly improves hepatic steatosis in patients with MASLD with no significant side effects.[14,15] In addition to blocking the final step of TG synthesis, the resulting suppression of SREBP-1 cleavage by DGAT2 inhibitors could have a clinical benefit beyond TG lowering because SREBP-1 is the only known transcriptional activator of *PNPLA3*.[65] A single-nucleotide polymorphism that results in a single amino acid change in *PNPLA3* (I148M) is strongly associated with increased liver TG, fibrosis, cirrhosis, and hepatocellular carcinoma.[66] *PNPLA3* (I148M) is a common variant found with frequencies that are concordant with the relative prevalence of MASLD in the three ancestry groups,[67] with the highest frequency in Hispanics (0.49) and lower frequencies in European Americans (0.23) and African Americans (0.17).[68] Inasmuch as DGAT2 inhibition suppresses SREBP-1 and PNPLA3 expression, this treatment modality may be uniquely beneficial to those who carry the PNPLA variant. Future clinical trials will be needed to determine whether carriers of the PNPLA variant or all individuals with MASLD benefit from DGAT2 inhibition.

Limitations of the study

We used multiple *in vitro* studies, animal models, and a DGAT2 inhibitor to show that changes in ER PE levels regulate SREBP-1 cleavage. Ideally, we would have liked to include an *in vivo* study where PE synthesis is specifically inhibited to show that lowering PE levels in this way also alters SREBP-1 cleavage. Unfortunately, specific inhibition of PE synthesis could not be achieved because PE levels can be altered through multiple metabolic pathways in liver. A second limitation was in our liposome-loading experiments using rat primary hepatocytes that demonstrated altering PE levels in the ER-regulated SREBP-1 activation. We would have liked to show in this system that the regulation was specific for SREBP-1 and not SREBP-2, but we did not have an antibody that recognized rat SREBP-2. However, we did show nSREBP-2 was not changed in our other *in vitro* and *in vivo* studies. Finally, because the primary purpose of the study was to use DGAT2 inhibition as a tool to further explore mechanisms that regulate SREBP-1 activation and thus lipogenesis in liver, we did not pursue additional studies to further dissect the relative importance of DGAT2 inhibition and SREBP-1 activation in mice treated with a MASH-inducing diet, although this question will be determined by the results of clinical trials using the DGAT2 inhibitor in individuals with MASH that are currently underway.

STAR★METHODS

RESOURCE AVAILABILITY

Lead contact—Further information and requests for resources and reagents should be directed to and will be fulfilled by the lead contact, Jay D. Horton (jay.horton@utsouthwestern.edu).

Materials availability—All unique reagents generated in this study are available from the lead contact with a completed materials transfer agreement.

Data and code availability

- All single cell sequencing data was deposited into GEO repository with GEO accession number: GSE250338. A PDF file with uncropped high-resolution scans of all the immunoblots presented in the paper, and an Excel file with the values that were used to create all graphs in the paper are included in ‘‘Data S1-Source Data.’’
- This paper does not report original code.
- Any additional information required to reanalyze the data reported in this paper is available from the lead contact upon request.

EXPERIMENTAL MODEL AND STUDY PARTICIPANT DETAILS

Animals—Study animals were maintained on a 12-h light/12-h dark cycle with free access to water and food (Teklad 2016 for rats and Teklad 2018 for mice). Unless otherwise noted, all animals were sacrificed at the beginning of the light cycle ~6:30 a.m. For the *ob/ob* mouse studies, mice were fasted for 2 hours (6:00 am-8:00 am) before sacrifice. Body weights and liver weights were recorded. Plasma and liver tissues were collected and subjected to further analysis or snap-frozen and stored at −80°C for future analysis. All animal experiments were performed with the approval of the Institutional Animal Care and Use Committee at the University of Texas Southwestern Medical Center.

Studies using the DGAT2 inhibitor were performed with C57BL/6J mice (Stock# 000664, Jackson Laboratory, USA), *ob/ob* mice (B6.Cg-Lep^{ob}/J, Stock# 000632, Jackson Laboratory, USA), or TghSREBP-1c rats[36] at ages of 9–11 weeks old. Animals were housed in shared chambers (3 mice in each chamber; 2 rats in each chamber) and were fed a powdered chow diet for 7 days before adding the iDgat2 to habituate the diet. Then the animals were fed the powdered chow diet, or a powdered chow mixed with iDgat2 (Sigma-Aldrich, Cat# PZ0233) at a concentration of 0.004% for mice or 0.01% for rats for 7 days before analysis. Food consumption in each chamber was recorded each day at 6:30 am. The food intake was calculated by dividing the average food consumption during the 7 days by the number of animals in each chamber.

In the DGAT2 overexpression studies, mouse *Dgat2* (NM_026384) was cloned to a pAAVscCB6 (p1023 G10) plasmid and sent to the Gene Therapy Center at University of Massachusetts Medical School for scAAV8.CB6-mDgat2 production. 5×10^{11} GC of

the scAAV8.CB6-mDgat2 or AAV-DJ-eGFP (VectorBiolabs, Cat# 7118) was injected into 8-week-old C57Bl/6J mice. Mice were housed for 5 additional weeks and fed the chow diet after the AAV injection and were then switched to a fat-free diet (MP biomedicals, Cat# 960238) for one week before samples were collected for study.

In the DGAT2, Insig-1 and Insig-2 knockout mice study, control scramble sgRNA or sgRNAs specific for mouse *Dgat2*, *Insig-1* and *Insig-2* were designed through CRISPick program developed by the Broad Institute (https://portals.broadinstitute.org/gppx/crispick/public). The sequences of the sgRNAs (Dgat2sg-F/R, Insig-1sg-F/R, Insig-2sg-F/R, and Scramble-F/R) are summarized in the key resources table. The sgRNAs were packaged into AAV-DJ vectors and AAVs were cultured with CRL3022 cells (HEK293S GnTI). The purified AAVs were injected into 8-week-old Cas9 knockin mice (B6J.129(Cg)-Gt(ROSA)26Sor$^{tm1.1(CAG-cas9*,-EGFP)Fezh}$/J Stock# 026179, Jackson laboratory, USA) at a dose of 1×10^{12} GC for each mouse. The mice were housed for 6 weeks after the injection before study.

For mice used to test AAV8 and AAV-DJ tissue and cell expression specificity, AAV8 and AAV-DJ expressing GFP or mCherry were generated. To generate the AAV-DJ virus expressing GFP, pAAV-CAG-shuttle-WPRE-GFP (Applied Viromics, plasmid# 0916), pAAV-DJ, and pHelper plasmids (Cell Biolabs, VPK-410-DJ) were co-transfected into CRL-3022 cells. To generate the AAV8 and AAV-DJ viruses expressing mCherry, the GFP gene within pAAV-CAG-shuttle-WPRE-GFP plasmid was replaced with mCherry via restriction enzyme digestion and ligation. Subsequently, the shuttle vector was co-transfected with pAAV8 (Addgene plasmid # 112864) or pAAV-DJ and pHelper plasmids into CRL3022 cells to produce AAV virus particles. Purification of AAV particles was performed 5 days after transfection.[69–71]

To determine the tissue specificity of AAV8 and AAV-DJ protein expression, AAV8-mCherry or AAV-DJ-mCherry (1×10^{12} GC for each mouse) was injected into C57Bl/6J mice. The mice were sacrificed 3 weeks after the injection and various tissues were collected for immunoblot analysis of mCherry protein. To test the liver cell type AAV8 and AAV-DJ expression, AAV-DJ-GFP and AAV8-mCherry viruses were mixed (1×10^{12} GC for each virus) and injected into C57Bl/6J mice. The mice were sacrificed 3 weeks after the injection for single cell RNA sequencing of liver.

Cell lines—Cell lines were maintained in the Cell Culture Core Facility of the Department of Molecular Genetics in UT Southwestern Medical Center. Hepa1c1c7 cells were maintained in a 37°C incubator with 5% CO_2. SV589 cells were maintained in a 37°C incubator with 5% CO_2. Unless otherwise noted, the cells were cultured in DMEM medium with 1g/L glucose supplemented with 5% FCS, 100 units/ml penicillin, and 100 μg/ml streptomycin sulfate). Detailed cell line information is summarized in the key resources table.

Deletion of *Insig-1* and *Insig-2* in SV589 cells—*Insig-1* and *Insig-2* were deleted from human fibroblast SV-589 cells using CRISPR-Cas9 technology. Briefly, oligonucleotide pairs encoding the indicated nucleotide guide sequences (OL1243/OL1244,

OL1247/OL1248 for Insig-1 and OL1515/OL1516, OL1517/OL1518 for Insig-2, sequence listed in key resources table) that target *Insig-1* and *Insig-2* were each annealed and cloned into the pX459 v2.0 plasmid (Addgene). All four plasmids were co-transfected into SV-589 cells using FuGENE 6. The transfected cells were subjected to selection with 1 μg/ml puromycin for two weeks. Single surviving colonies were picked, expanded, and screened by PCR followed by sequencing. Single-cell clones were isolated by limiting dilution to establish the Insig-1 and Insig-2 double knockout cell line (TR4410).

Materials—Information of materials used in this study is summarized in the key resources table.

METHOD DETAILS

Plasma and liver biochemical measurements—Plasma cholesterol, TGs, glucose, and liver lipid concentrations were measured by the Metabolic Phenotyping Core at UT South-western Medical Center as described previously.[33] Plasma insulin was measured using an ultra-sensitive insulin ELIAS kit (Crystal Chem, USA).

Liver cell isolation and Single cell RNA sequencing—Hepatocytes and non-parenchymal liver cells were isolated using Liberase digestion. The mouse was euthanized by isoflurane inhalation, the IVC was cannulated with an 18-gauge catheter, and the hepatic vein was cut for perfusion. The liver was perfused with liver cleaning buffer (HBSS, − Ca^{2+}, − Mg^{2+}, no phenol red, 0.5mM EGTA, 0.75mM EDTA, 20mM HEPES, 1μM flavopiridol) followed by digestion buffer (HBSS, + Ca^{2+}, + Mg^{2+}, no phenol red, 0.1 mg/ml liberase, 20 μg/ml DNase 1, 20mM HEPES, 1 μM flavopiridol) at a rate of 5 ml/min. After perfusion, the liver was removed and placed in a 50 ml conical tube containing digestion buffer for further tissue dissociation by pipetting. The tissue mixture was incubated at 37°C for an additional 20 min and then strained through a 100 μm cell strainer into a 50 ml conical tube containing 20 ml of Wash buffer. The mixture was centrifuged at 500 g for 3 min and the supernatant was collected and transferred to a 20% Percoll solution. This mixture was centrifuged at 600 g for 15 min and the supernatant was aspirated and discarded. The pellet was washed with 20 ml of the wash buffer (HBSS, + Ca^{2+},+ Mg^{2+}, no phenol red, 20 μg/ml DNase 1, 2% FBS, 20mM HEPES), centrifuged at 500 g for 7 min and resuspended in 10 ml of 28% OptiPrep density gradient solution.

To assemble the gradient, cells suspended in 28% OptiPrep density gradient solution were transferred into a 15 ml conical tube containing 3 ml Wash buffer. The gradient solution was centrifuged at 1,400 g for 25 min (centrifuge acceleration set to 3, and deceleration to 0). After gradient centrifugation, the cell pellet was resuspended in 1 ml RBC lysis buffer and incubated on ice for 5 min. 10 ml pre-chilled PBS buffer was then added to the RBC lysis buffer containing the cell pellet. The mixture was centrifuged at 400 g for 7 min and the pellet was mixed with 1 ml chilled PBS buffer for cell counting. The approximate cell viability was 90%, as determined by trypan blue staining. The final single cell suspension was used to generate separate libraries via 10X Genomics Chromium Single Cell 3’ Library and Gel Beads Kit (version 3). The detailed single cell sequencing protocol was previously described.[72] New custom mice gene reference genomes were created by adding both GFP

and mCherry into existing mouse gene reference genomes ‘‘refdata-gex-mm10-2020-A’’. Addition of GFP and mCherry marker genes to the available mouse gene reference was achieved via 10× Genomics instructions (https://support.10xgenomics.com/single-cell-gene-expression/software/pipelines/latest/using/tutorial_mr).

GFP gene (1328 bp)
: atggtgagcaagcagatcctgaagaacaccggcctgcaggagatcatgagcttcaaggtgaacctggagggcgtggtgaacaaccacgtgttcaccatggagggc

CHERRY gene (1354 bp)
: atggtgagcaagggcgaggaggataacatggccatcatcaaggagttcatgcgcttcaaggtgcacatggagggctccgtgaacggccacgagttcgagatcgag

The detailed single cell sequencing data analysis was previously described.[72] All single cell sequencing data was deposited into GEO repository with GEO accession number: GSE250338.

***In vivo* liver lipid secretion—**Male mice (n=5 for each group) were fed chow, or a chow mixed with iDgat2 at a concentration of 0.004% for 7 days. On Day 8, the mice were fasted for 4 hours (6 am-10 am), and 10% Triton WR-1339/saline solution (Tyloxapol; Sigma-Aldrich) (500 mg/kg body weight) was injected into mice intravenously. Blood was collected from the tail vein at 0, 0.5, 1, 1.5, 2, and 3 hours after the injection and plasma was separated for measurement of TG levels. The plasma TG secretion rate was calculated from the slope of the linear regression of the time vs. TG concentration.[33]

ER isolation—ER fractions were prepared from freshly collected liver samples using the following procedures. Liver tissue (~500 mg) was gently homogenized in ice-cold buffer A (50 mM Tris-HCl pH 7.5, 150 mM NaCl) with 15% sucrose using a 2 ml Dounce homogenizer. The homogenized liver tissue was centrifuged at 500 × g for 10 min to remove unhomogenized tissue debris. The supernatant was then centrifuged at 15,000 × g for 10 min and the supernatant was collected and overlayed on a discontinuous sucrose gradient (2 ml of 15%, 4 ml of 30%, and 2 ml of 45% of sucrose in buffer A). One ml of 7.5% sucrose was then layered on top of the samples. The gradient was centrifuged at 100,000 × g for 1 hour, and the fraction between 30% and 45% layers was collected and loaded to a second discontinuous sucrose gradient (2 ml of 45%, 4 ml of 51%, and 2 ml of 60% sucrose in buffer A). Two ml of 30% sucrose was then added to the top of the samples. The second gradient was centrifuged at 150,000 × g for 70 min. The samples between 30% and 45% layers were collected, mixed with 300 μl of 45% sucrose and loaded to the bottom of a third gradient containing 2.25 ml each of 19%, 21%, 23%, and 25% (v/v) iodixanol in buffer A. This gradient solution with sample was centrifuged for 2 hours at 110,000 × g and fractions (1 ml each) were collected from the bottom of the tube. The fractions from tubes 2–6 were pooled as ER fraction.

ER lipid analysis—Sterols and oxysterols in the ER fractions were measured using mass spectrometry as previously described.[73] Total phospholipid concentrations were determined using a colorimetric assay that measures inorganic phosphate released after

acid digestion and the value was used to calculate the molar percentage of cholesterol in the ER fraction.[74] Different phospholipid species in the ER were measured by LC-MS/MS. Briefly, ER samples were transferred to glass tubes with 1 ml each of methanol, water and dicloromethane. The mixture was vortexed, centrifuged, and the organic phase (bottom) was transferred to a fresh glass tube with a Pasteur pipette and 20 μl of 1:100 diluted SPLASH LipidoMix internal standard (Avanti Polar Lipids, Alabaster, AL) was added. The samples were dried under N_2 and resuspended in 400 μl of hexane. Lipids were analyzed by LC-MS/MS using a SCIEX QTRAP 6500+ (SCIEX, Framingham, MA) equipped with a Shimadzu LC-30AD (Shimadzu, Columbia, MD) high-performance liquid chromatography (HPLC) system and a 150 × 2.1 mm, 5μm Supelco Ascentis silica column (Supelco, Bellefonte, PA). Samples were injected at a flow rate of 0.3 ml/min at 2.5% solvent B (methyl tert-butyl ether) and 97.5% Solvent A (hexane). Solvent B was increased to 5% over 3 min and then to 60% over 6 min. Solvent B was reduced to 0% over 30 seconds while Solvent C (90:10 (v/v) Isopropanol-water) was set at 20% and increased to 40% during the following 11 min. Solvent C was increased to 44% over 6 min and then to 60% over 50 seconds. The system was held at 60% solvent C for 1 min prior to re-equilibration at 2.5% of solvent B for 5 min at a 1.2 ml/min flow rate. Solvent D (95:5 (v/v) acetonitrile-water with 10 mM Ammonium acetate) was infused post-column at 0.03 ml/min. Column oven temperature was 25°C. Data was acquired in positive and negative ionization mode using multiple reaction monitoring (MRM). The LC-MS/MS data was analyzed using MultiQuant software (SCIEX). Each lipid species data was normalized to its correspondent internal standard from the same lipid class and recorded as an arbitrary unit. The data was then normalized to the amount of ER protein used in the analysis. To compare different groups, the values in the control group was set as 1 and all other groups are shown as levels relative to the control group.

Quantitative real-time PCR—Total RNA was extracted from liver using RNA STAT-60 (Tel-Test). cDNA was synthesized from 2 μg of DNase I treated total RNA using a Taqman reverse transcription kits (Applied Biosystems, Carlsbad, CA). The quantitative real-time RT-PCR reaction included 20 ng of reverse-transcribed total RNA, 167 nM of the forward and reverse primers, and 10 μl of 2× SYBR Green PCR master Mix (Applied Biosystems, Carlsbad, CA). PCR reactions were carried out in 384-well plates using the ABI PRISM 7900HT Sequence Detection System (Applied Biosystems, Carlsbad, CA). All reactions were done in triplicate, and the relative amount of all mRNAs was calculated using the comparative threshold cycle method. Cyclophilin mRNA was used as invariant control. The sequence of primers used in the real-time PCR were summarized in the key resources table and Table S1.

Immunoblot analysis—Whole cell lysates from cultured cells or membrane and nuclear proteins from primary hepatocytes and frozen livers were prepared as described.[33,36] Individual samples were loaded on an 8% SDS-PAGE gel for immunoblot analysis of SREBPs or 4–20% gradient SDS-PAGE gels for immunoblot analysis of other proteins and transferred to a nitrocellulose membrane (Bio-Rad, Hercules, CA). Immunoblot analysis was performed using primary antibodies specific to each individual protein. Bounded antibodies were visualized using SuperSignal West Pico Chemiluminescent Substrate (ThermoFisher)

after incubation with HRP conjugated secondary antibodies (Goat anti-rabbit IgG or goat anti-mouse IgG). The images were scanned using an Odyssey FC Imager and analyzed using Image Studio version. 5.0 (LI-COR). SREBP-1 and SREBP-2 were detected using rabbit anti-SREBP-1 monoclonal (20B12), and rabbit anti-SREBP-2 monoclonal (22D5) antibody, respectively, as previously described.[33] TghSREBP-1c was detected using a rabbit anti-HA-Tag antibody (Cell Signaling). Mouse anti-CREB (cAMP response element binding protein, Invitrogen), rabbit anti-LSD1 (Cell Signaling), rabbit anti-β actin (Cell Signaling) and rabbit anti-Calnexin (Enzo Life Science) antibodies were used as loading controls for nuclear, cytosolic, and membrane proteins, respectively. In the animal studies, individual protein samples were prepared from liver and used for immunoblotting. The intensity of each bond on the blot was quantified with Image Studio software. The intensity of SREBPs was normalized to the loading controls (Calnexin for membrane control and LSD1 for nuclear control). The result was expressed as intensity relative to the control group. In the ER accessible cholesterol-ALOD4 binding study, rabbit anti-Calnexin antibody was mixed with mouse anti-His antibody as primary antibodies for immunoblotting. The mixture of Li-COR IRDY 800cw goat anti-rabbit IgG and Li-COR IRDY 680 goat anti-mouse IgG was used as secondary antibody to detect Calnexin and His-tagged ALOD4 respectively. For immunoblot analysis of fractions in the process of ER isolation, each ER fraction prepared at the step of ER fraction isolation was diluted 5-fold with buffer A and centrifuged at 150,000 × g for 1 hour. The pellet was resuspended and loaded to a 4–20% gradient precast protein gel (Bio-Rad) and transferred to a nitrocellulose membrane. Due to the limit amount of protein collected from the fractions, to avoid protein lost during multiple stripping, the membrane was cut to individual strips according to the molecular weight of the corresponding proteins. Immunoblot analyses were performed using antibodies against protein markers from different subcellular organelles. The individual membrane strips were placed back into an intact membrane and visualized using the Odyssey FC Imager to ensure the integrity of the membrane before obtaining the individual images. Detailed antibody information is listed in the key resources table.

Assays for accessible cholesterol in membranes—ER fractions were prepared as above and diluted 5-fold in buffer A and centrifuged for 1 hour at 150,000 × g. The ER fractions were resuspended in 300 μl of buffer A and 10 μg of the pelleted ER protein was used for the reaction. In one set of samples, the ER fraction was incubated with 3% (w/v) of hydroxypropyl-β-cyclodextrin (HPCD, ThermoFisher) for 30 min at room temperature to remove cholesterol in the ER fraction and served as a negative control. Another set of samples was incubated in an identical fashion without the addition of HPCD. After the respective treatments, 3 μM of His-tagged ALOD4 in buffer A was added to all the samples, incubated at room temperature for 30 min, and the ER fraction was collected by centrifugation at 50,000 × g for 30 min. The pelleted ER fractions and supernatants were subjected to a 4–20% gradient precast protein gel (Bio-Rad) and transferred to a nitrocellulose membrane. The binding of ALOD4 to the ER fraction was evaluated by immunoblot analysis using an anti-His antibody that recognizes the His-tagged ALOD4.[47,48]

Preparation of PE containing liposomes—ER targeting liposomes were prepared as described.[52,53] Briefly, 1 μmol of total phospholipids was mixed with the molar ratio

as indicated: control (No PE or PC), PI:PS= 0.2 μmol: 0.2 μmol; low PE, PE:PC:PI:PS= 0.1 μmol: 0.5 μmol: 0.2 μmol:0.2 μmol; high PE, PE:PC:PI:PS= 0.5 μmol: 0.1 μmol: 0.2 μmol: 0.2 μmol, dried down and vacuumed for 30 min. The dried phospholipid mixture was rehydrated in 1ml of PBS at 55°C for 30 min with vigorous vortex. The solution was then passed through a 0.1 μm polycarbonate membrane 10 times using a mini-Extruder (Avanti lipids, Cat # 610000) to form unilaminar liposomes.

Liposome supplementation—Cells were seeded in 100 mm dishes with DMEM (1 g/L glucose, 5% FCS) for 2 hours (primary hepatocyte) or overnight (Hepa-1c1c7) in the 37°C incubate with 5% CO_2. Medium was then replaced with high glucose DMEM (2.5 g/L glucose, 5% lipoprotein-deficient serum) containing 50 μM of control, low PE or high PE liposomes and incubated for 3 hours. 25 μg/ml of ALLN was added 30 min before cells were harvested for analysis.

Ethanolamine supplementation to SV589 cells—On day 0, control SV589 cells and Insig knockout cells (TR4410) were set up in DMEM (1 g/L glucose, 5% FCS). In the afternoon of day 1, the cells were changed to culture medium (DMEM, 1 g/L glucose, 5% lipoprotein-deficient serum) containing 100 μM of palmitate or 100 μM of ethanolamine or 100 μM of both palmitate and ethanolamine. All culture medium was adjusted to contain 0.35% BSA. In the early morning of day 2, 25 μg/ml of ALLN was added to the cells. Cells were harvested 2 hours later for SREBP-1 and SREBP-2 immunoblot analysis.

Vesicle budding assay—The liver vesicle budding assay was modified based on the previously published protocols.[75–77] C57Bl/6J mice fed chow were anesthetized by inhalation of isoflurane. Livers were perfused with saline (0.9% NaCl) for 10 min at a rate of 5 ml/min. 500 mg of the perfused livers were then homogenized in 1 ml of buffer C (50 mM HEPES-KOH at pH 7.2, 250 mM sorbitol, 70 mM potassium acetate, 5 mM EGTA, 2.5 mM magnesium acetate plus protease inhibitors). Homogenates were sequentially centrifuged at 1000 g for 10 min, 20,000 g for 20 min, 186,000 g for 1 hour, and 186,000 g for 45 min. Supernatants from each spin were transferred to new tubes for the subsequent centrifugation. After the final spin, the protein concentrations of the supernatants were determined by BCA (13.5 mg/ml) and stored in −80°C as liver cytosol for use in the vesicle budding assay below.

Liver samples (200 mg) were homogenized in 1 ml of buffer B (10 mM HEPES-KOH at pH 7.2, 250 mM sorbitol, 10 mM potassium acetate, 1.5 mM magnesium acetate plus protease inhibitors) with a loose Dounce homogenizer. The homogenates were centrifuged twice at 1500 g for 5 min at 4°C to remove tissue debris and the nuclear fractions. The supernatants were then centrifuged at 16,000 g for 5 min. Pellets from the spin were resuspended in 500 μl of buffer C, then centrifuged at 16,000 g for 5 min. The supernatants were removed, and the pellets were resuspended in 70 μl of buffer C as liver microsomes. Protein concentrations were determined by BCA. The vesicle budding assay was performed in a final volume of 80 μl with equal amount of microsomes mixed with 1.5 mM ATP, 0.5 mM GTP, 10 mM creatine phosphate, 5 units/ml of creatine kinase, and 135 μg of mouse cytosol prepared as described in the previous paragraph. The reactions were carried out at 37°C for 20 min, placed on ice for 5 min, and then centrifuged at 16,000 g for 3 min. The pellets were resuspended in SDS-lysis buffer as microsomes. The vesicles formed during the budding

assay in the supernatants were pelleted by ultracentrifugation at 137,000 g for 30 min and resuspended in SDS-lysis buffer. The microsomes and vesicles were mixed with 5× SDS-loading buffer and incubated in 37°C for 20 min before subjected to an 8% SDS-PAGE for immunoblot analysis.

QUANTIFICATION AND STATISTICAL ANALYSIS

The images of the immunoblots were scanned using an Odyssey FC Imager and the binding of antibodies to the specific proteins were quantified using Image Studio version. 5.0 (LI-COR). Statistical analysis was performed using GraphPad Prism. Data was compared using an unpaired two-tailed Student's *t*-test. Significant levels were set at $p<0.05$, $p<0.01$ or $p<0.001$ as described on figure legends.

Supplementary Material

Refer to Web version on PubMed Central for supplementary material.

ACKNOWLEDGMENTS

We thank Norma Anderson, Judy Sanchez, Tuyet Dang, Samuel Purkey, and Tessa Edwards for excellent technical assistance and Chelsea Burroughs and Nancy Heard for assistance with graphics. The work is supported by grants NIH P01HL-160487 and NIH P30DK127984 to J.D.H.; grant UL1TR003163 to J.G.M.; NIH AI-158357, the Welch Foundation (I-1793), and the Leducq Foundation (19CVD04) to A.R.; and the Science and Technology Commission of Shanghai Municipality (23ZR1411000) to M.X.

REFERENCES

1. Rinella ME, Lazarus JV, Ratziu V, Francque SM, Sanyal AJ, Kanwal F, Romero D, Abdelmalek MF, Anstee QM, Arab JP, et al. (2023). A multi-society Delphi consensus statement on new fatty liver disease nomenclature. Hepatology 78, 1966–1986. [PubMed: 37363821]
2. Angulo P (2002). Nonalcoholic fatty liver disease. N. Engl. J. Med 346, 1221–1231. [PubMed: 11961152]
3. Browning JD, and Horton JD (2004). Molecular mediators of hepatic steatosis and liver injury. J. Clin. Invest 114, 147–152. [PubMed: 15254578]
4. Sanyal A, Poklepovic A, Moyneur E, and Barghout V (2010). Population-based risk factors and resource utilization for HCC: US perspective. Curr. Med. Res. Opin 26, 2183–2191. [PubMed: 20666689]
5. Younossi Z, Tacke F, Arrese M, Sharma BC, Mostafa I, Bugianesi E, Wong VW, Yilmaz Y, George J, Fan J, and Vos MB (2018). Global Perspectives on Non-alcoholic Fatty Liver Disease and Non-alcoholic Steatohepatitis. Hepatology 4, 30251.
6. Cohen JC, Horton JD, and Hobbs HH (2011). Human fatty liver disease: old questions and new insights. Science 332, 1519–1523. [PubMed: 21700865]
7. Dongiovanni P, Stender S, Pietrelli A, Mancina RM, Cespiati A, Petta S, Pelusi S, Pingitore P, Badiali S, Maggioni M, et al. (2018). Causal relationship of hepatic fat with liver damage and insulin resistance in nonalcoholic fatty liver. J. Intern. Med 283, 356–370. [PubMed: 29280273]
8. Pelusi S, and Valenti L (2019). Hepatic fat as clinical outcome and therapeutic target for nonalcoholic fatty liver disease. Liver Int 39, 250–256. [PubMed: 30248234]
9. Lambert JE, Ramos-Roman MA, Browning JD, and Parks EJ (2014). Increased de novo lipogenesis is a distinct characteristic of individuals with nonalcoholic fatty liver disease. Gastroenterology 146, 726–735. [PubMed: 24316260]
10. Kim CW, Addy C, Kusunoki J, Anderson NN, Deja S, Fu X, Burgess SC, Li C, Ruddy M, Chakravarthy M, et al. (2017). Acetyl CoA Carboxylase inhibition reduces hepatic steatosis but

elevates plasma triglycerides in mice and humans: A bedside to bench investigation. Cell Metab 26, 394–406.e396. [PubMed: 28768177]

11. Pinkosky SL, Groot PHE, Lalwani ND, and Steinberg GR (2017). Targeting ATP-Citrate Lyase in Hyperlipidemia and Metabolic Disorders. Trends Mol. Med 23, 1047–1063. [PubMed: 28993031]
12. Goedeke L, Bates J, Vatner DF, Perry RJ, Wang T, Ramirez R, Li L, Ellis MW, Zhang D, Wong KE, et al. (2018). Acetyl-CoA Carboxylase Inhibition Reverses NAFLD and Hepatic Insulin Resistance but Promotes Hypertriglyceridemia in Rodents. Hepatology 68, 2197–2211. [PubMed: 29790582]
13. Loomba R, Mohseni R, Lucas KJ, Gutierrez JA, Perry RG, Trotter JF, Rahimi RS, Harrison SA, Ajmera V, Wayne JD, et al. (2021). TVB-2640 (FASN Inhibitor) for the Treatment of Nonalcoholic Steatohepatitis: FASCINATE-1, a Randomized, Placebo-Controlled Phase 2a Trial. Gastroenterology 161, 1475–1486. [PubMed: 34310978]
14. Amin NB, Carvajal-Gonzalez S, Purkal J, Zhu T, Crowley C, Perez S, Chidsey K, Kim AM, and Goodwin B (2019). Targeting diacylglycerol acyltransferase 2 for the treatment of nonalcoholic steatohepatitis. Sci. Transl. Med 11, eaav9701. [PubMed: 31776293]
15. Calle RA, Amin NB, Carvajal-Gonzalez S, Ross TT, Bergman A, Aggarwal S, Crowley C, Rinaldi A, Mancuso J, Aggarwal N, et al. (2021). ACC inhibitor alone or co-administered with a DGAT2 inhibitor in patients with non-alcoholic fatty liver disease: two parallel, placebo-controlled, randomized phase 2a trials. Nat. Med 27, 1836–1848. [PubMed: 34635855]
16. Yen CL, Stone SJ, Koliwad S, Harris C, and Farese RV Jr. (2008). Thematic review series: glycerolipids. DGAT enzymes and triacylglycerol biosynthesis. Thematic Review Series. J. Lipid Res 49, 2283–2301. [PubMed: 18757836]
17. Lardizabal KD, Mai JT, Wagner NW, Wyrick A, Voelker T, and Hawkins DJ (2001). DGAT2 is a new diacylglycerol acyltransferase gene family: purification, cloning, and expression in insect cells of two polypeptides from Mortierella ramanniana with diacylglycerol acyltransferase activity. J. Biol. Chem 276, 38862–38869. [PubMed: 11481333]
18. Cases S, Smith SJ, Zheng Y-W, Myers HM, Lear SR, Sande E, Novak S, Collins C, Welch CB, Lusis AJ, et al. (1998). Identification of a gene encoding an acyl CoA:diacylglycerol acyltransferase, a key enzyme in triacylglycerol synthesis. Proc. Natl. Acad. Sci. USA 95, 13018–13023. [PubMed: 9789033]
19. Cases S, Stone SJ, Zhou P, Yen E, Tow B, Lardizabal KD, Voelker T, and Farese RV Jr. (2001). Cloning of DGAT2, a second mammalian diacylglycerol acyltransferase, and related family members. J. Biol. Chem 276, 38870–38876. [PubMed: 11481335]
20. Villanueva CJ, Monetti M, Shih M, Zhou P, Watkins SM, Bhanot S, and Farese RV Jr. (2009). Specific role for acyl CoA:Diacylglycerol acyltransferase 1 (Dgat1) in hepatic steatosis due to exogenous fatty acids. Hepatology 50, 434–442. [PubMed: 19472314]
21. Wurie HR, Buckett L, and Zammit VA (2012). Diacylglycerol acyltransferase 2 acts upstream of diacylglycerol acyltransferase 1 and utilizes nascent diglycerides and de novo synthesized fatty acids in HepG2 cells. FEBS Journal 279, 3033–3047. [PubMed: 22748069]
22. Gluchowski NL, Gabriel KR, Chitraju C, Bronson RT, Mejhert N, Boland S, Wang K, Lai ZW, Farese RV Jr., and Walther TC (2019). Hepatocyte deletion of triglyceride-synthesis enzyme acyl CoA: diacylglycerol acyltransferase 2 reduces steatosis without increasing inflammation or fibrosis in mice. Hepatology 70, 1972–1985. [PubMed: 31081165]
23. Yu XX, Murray SF, Pandey SK, Booten SL, Bao D, Song XZ, Kelly S, Chen S, McKay R, Monia BP, and Bhanot S (2005). Antisense oligonucleotide reduction of DGAT2 expression improves hepatic steatosis and hyperlipidemia in obese mice. Hepatology 42, 362–371. [PubMed: 16001399]
24. Choi CS, Savage DB, Kulkarni A, Yu XX, Liu ZX, Morino K, Kim S, Distefano A, Samuel VT, Neschen S, et al. (2007). Suppression of diacylglycerol acyltransferase-2 (DGAT2), but not DGAT1, with antisense oligonucleotides reverses diet-induced hepatic steatosis and insulin resistance. J. Biol. Chem 282, 22678–22688. [PubMed: 17526931]
25. Monetti M, Levin MC, Watt MJ, Sajan MP, Marmor S, Hubbard BK, Stevens RD, Bain JR, Newgard CB, Farese RV Sr., et al. (2007). Dissociation of hepatic steatosis and insulin resistance in mice overexpressing DGAT in the liver. Cell Metab 6, 69–78. [PubMed: 17618857]

26. Yenilmez B, Wetoska N, Kelly M, Echeverria D, Min K, Lifshitz L, Alterman JF, Hassler MR, Hildebrand S, DiMarzio C, et al. (2022). An RNAi therapeutic targeting hepatic DGAT2 in a genetically obese mouse model of nonalcoholic steatohepatitis. Mol. Ther 30, 1329–1342. [PubMed: 34774753]
27. Brown MS, and Goldstein JL (2009). Cholesterol feedback: from Schoenheimer's bottle to Scap's MELADL. J. Lipid Res 50, S15–S27. [PubMed: 18974038]
28. Horton JD, Goldstein JL, and Brown MS (2002). SREBPs:activators of the complete program of cholesterol and fatty acid synthesis in the liver. J. Clin. Invest 109, 1125–1131. [PubMed: 11994399]
29. Shimomura I, Shimano H, Korn BS, Bashmakov Y, and Horton JD (1998). Nuclear sterol regulatory element-binding proteins activate genes responsible for the entire program of unsaturated fatty acid biosynthesis in transgenic mouse liver. J. Biol. Chem 273, 35299–35306. [PubMed: 9857071]
30. Moon YA, Liang G, Xie X, Frank-Kamenetsky M, Fitzgerald K, Koteliansky V, Brown MS, Goldstein JL, and Horton JD (2012). The Scap/SREBP pathway is essential for developing diabetic fatty liver and carbohydrate-induced hypertriglyceridemia in animals. Cell Metab 15, 240–246. [PubMed: 22326225]
31. Yang T, Espenshade PJ, Wright ME, Yabe D, Gong Y, Aebersold R, Goldstein JL, and Brown MS (2002). Crucial step in cholesterol homeostasis:sterols promote binding of SCAP to INSIG-1, a membrane protein that facilitates retention of SREBPs in ER. Cell 110, 489–500. [PubMed: 12202038]
32. Futatsugi K, Kung DW, Orr ST, Cabral S, Hepworth D, Aspnes G, Bader S, Bian J, Boehm M, Carpino PA, et al. (2015). Discovery and Optimization of Imidazopyridine-Based Inhibitors of Diacylglycerol Acyltransferase 2 (DGAT2). J. Med. Chem 58, 7173–7185. [PubMed: 26349027]
33. Rong S, Cortés VA, Rashid S, Anderson NN, McDonald JG, Liang G, Moon YA, Hammer RE, and Horton JD (2017). Expression of SREBP-1c requires SREBP-2-mediated generation of a sterol ligand for LXR in livers of mice. eLife 6, e25015. [PubMed: 28244871]
34. Repa JJ, Liang G, Ou J, Bashmakov Y, Lobaccaro JM, Shimomura I, Shan B, Brown MS, Goldstein JL, and Mangelsdorf DJ (2000). Regulation of mouse sterol regulatory element-binding protein-1c gene (SREBP-1c) by oxysterol receptors, LXRa and LXRb. Genes Dev 14, 2819–2830. [PubMed: 11090130]
35. Amemiya-Kudo M, Shimano H, Yoshikawa T, Yahagi N, Hasty AH, Okazaki H, Tamura Y, Shionoiri F, Iizuka Y, Ohashi K, et al. (2000). Promoter analysis of the mouse sterol regulatory element-binding protein-1c gene. J. Biol. Chem 275, 31078–31085. [PubMed: 10918064]
36. Owen JL, Zhang Y, Bae SH, Farooqi MS, Liang G, Hammer RE, Goldstein JL, and Brown MS (2012). Insulin stimulation of SREBP-1c processing in transgenic rat hepatocytes requires p70 S6-kinase. Proc. Natl. Acad. Sci. USA 109, 16184–16189. [PubMed: 22927400]
37. Brown MS, and Goldstein JL (1997). The SREBP pathway: regulation of cholesterol metabolism by proteolysis of a membrane-bound transcription factor. Cell 89, 331–340. [PubMed: 9150132]
38. Wang X, Sato R, Brown MS, Hua X, and Goldstein JL (1994). SREBP-1, a membrane-bound transcription factor released by sterol-regulated proteolysis. Cell 77, 53–62. [PubMed: 8156598]
39. Gao Y, Zhou Y, Goldstein JL, Brown MS, and Radhakrishnan A (2017). Cholesterol-induced conformational changes in the sterol-sensing domain of the Scap protein suggest feedback mechanism to control cholesterol synthesis. J. Biol. Chem 292, 8729–8737. [PubMed: 28377508]
40. Infante RE, and Radhakrishnan A (2017). Continuous transport of a small fraction of plasma membrane cholesterol to endoplasmic reticulum regulates total cellular cholesterol. eLife 6, e25466. [PubMed: 28414269]
41. Radhakrishnan A, Goldstein JL, McDonald JG, and Brown MS (2008). Switch-like control of SREBP-2 transport triggered by small changes in ER cholesterol: a delicate balance. Cell Metab 8, 512–521. [PubMed: 19041766]
42. Radhakrishnan A, Ikeda Y, Kwon HJ, Brown MS, and Goldstein JL (2007). Sterol-regulated transport of SREBPs from endoplasmic reticulum to Golgi: oxysterols block transport by binding to Insig. Proc. Natl. Acad. Sci. USA 104, 6511–6518. [PubMed: 17428920]

43. Radhakrishnan A, Sun LP, Kwon HJ, Brown MS, and Goldstein JL (2004). Direct binding of cholesterol to the purified membrane region of SCAP: mechanism for a sterol-sensing domain. Mol. Cell 15, 259–268. [PubMed: 15260976]
44. Sokolov A, and Radhakrishnan A (2010). Accessibility of cholesterol in endoplasmic reticulum membranes and activation of SREBP-2 switch abruptly at a common cholesterol threshold. J. Biol. Chem 285, 29480–29490. [PubMed: 20573965]
45. Zhang Y, Lee KM, Kinch LN, Clark L, Grishin NV, Rosenbaum DM, Brown MS, Goldstein JL, and Radhakrishnan A (2016). Direct Demonstration That Loop1 of Scap Binds to Loop7: A crucial event in cholesterol homeostasis. J. Biol. Chem 291, 12888–12896. [PubMed: 27068746]
46. Das A, Brown MS, Anderson DD, Goldstein JL, and Radhakrishnan A (2014). Three pools of plasma membrane cholesterol and their relation to cholesterol homeostasis. eLife 3.
47. Gay A, Rye D, and Radhakrishnan A (2015). Switch-like responses of two cholesterol sensors do not require protein oligomerization in membranes. Biophys. J 108, 1459–1469. [PubMed: 25809258]
48. Johnson KA, and Radhakrishnan A (2021). The use of anthrolysin O and ostreolysin A to study cholesterol in cell membranes. Methods Enzymol 649, 543–566. [PubMed: 33712199]
49. Shimomura I, Bashmakov Y, and Horton JD (1999). Increased levels of nuclear SREBP-1c associated with fatty livers in two mouse models of diabetes mellitus. J. Biol. Chem 274, 30028–30032. [PubMed: 10514488]
50. Clark AJ, and Block K (1959). The absence of sterol synthesis in insects. J. Biol. Chem 234, 2578–2582. [PubMed: 13810427]
51. Dobrosotskaya IY, Seegmiller AC, Brown MS, Goldstein JL, and Rawson RB (2002). Regulation of SREBP processing and membrane lipid production by phospholipids in drosophila. Science 296, 879–883. [PubMed: 11988566]
52. Pollock S, Antrobus R, Newton L, Kampa B, Rossa J, Latham S, Nichita NB, Dwek RA, and Zitzmann N (2010). Uptake and trafficking of liposomes to the endoplasmic reticulum. FASEB J 24, 1866–1878. [PubMed: 20097877]
53. Rong X, Wang B, Palladino EN, de Aguiar Vallim TQ, Ford DA, and Tontonoz P (2017). ER phospholipid composition modulates lipogenesis during feeding and in obesity. J. Clin. Invest 127, 3640–3651. [PubMed: 28846071]
54. Kent C (1995). Eukaryotic phospholipid biosynthesis. Annu. Rev. Biochem 64, 315–343. [PubMed: 7574485]
55. Jo Y, Lee PC, Sguigna PV, and DeBose-Boyd RA (2011). Sterol-induced degradation of HMG CoA reductase depends on interplay of two Insigs and two ubiquitin ligases, gp78 and Trc8. Proc. Natl. Acad. Sci. USA 108, 20503–20508. [PubMed: 22143767]
56. Engelking LJ, Kuriyama H, Hammer RE, Horton JD, Brown MS, Goldstein JL, and Liang G (2004). Overexpression of Insig-1 in the livers of transgenic mice inhibits SREBP processing and reduces insulin-stimulated lipogenesis. J. Clin. Invest 113, 1168–1175. [PubMed: 15085196]
57. McFarlane MR, Liang G, and Engelking LJ (2014). Insig proteins mediate feedback inhibition of cholesterol synthesis in the intestine. J. Biol. Chem 289, 2148–2156. [PubMed: 24337570]
58. Adams CM, Reitz J, De Brabander JK, Feramisco JD, Li L, Brown MS, and Goldstein JL (2004). Cholesterol and 25-hydroxycholesterol inhibit activation of SREBPs by different mechanisms, both involving SCAP and Insigs. J. Biol. Chem 279, 52772–52780. [PubMed: 15452130]
59. Seegmiller AC, Dobrosotskaya I, Goldstein JL, Ho YK, Brown MS, and Rawson RB (2002). The SREBP pathway in Drosophila: regulation by palmitate, not sterols. Dev. Cell 2, 229–238. [PubMed: 11832248]
60. Zambrano F, Fleischer S, and Fleischer B (1975). Lipid composition of the Golgi apparatus of rat kidney and liver in comparison with other subcellular organelles. Biochim. Biophys. Acta 380, 357–369. [PubMed: 1169965]
61. Moon YA, Hammer RE, and Horton JD (2009). Deletion of ELOVL5 leads to fatty liver through activation of SREBP-1c in mice. J. Lipid Res 50, 412–423. [PubMed: 18838740]
62. Hannah VC, Ou J, Luong A, Goldstein JL, and Brown MS (2001). Unsaturated fatty acids down-regulate SREBP isoforms 1a and 1c by two mechanisms in HEK-293 cells. J. Biol. Chem 276, 4365–4372. [PubMed: 11085986]

63. Horton JD, Bashmakov Y, Shimomura I, and Shimano H (1998). Regulation of sterol regulatory element binding proteins in livers of fasted and refed mice. Proc. Natl. Acad. Sci. USA 95, 5987–5992. [PubMed: 9600904]
64. Shimomura I, Bashmakov Y, Ikemoto S, Horton JD, Brown MS, and Goldstein JL (1999). Insulin selectively increases SREBP-1c mRNA in the livers of rats with streptozotocin-induced diabetes. Proc. Natl. Acad. Sci. USA 96, 13656–13661. [PubMed: 10570128]
65. Huang Y, He S, Li JZ, Seo YK, Osborne TF, Cohen JC, and Hobbs HH (2010). A feed-forward loop amplifies nutritional regulation of PNPLA3. Proc. Natl. Acad. Sci. USA 107, 7892–7897. [PubMed: 20385813]
66. Singal AG, Manjunath H, Yopp AC, Beg MS, Marrero JA, Gopal P, and Waljee AK (2014). The Effect of PNPLA3 on Fibrosis Progression and Development of Hepatocellular Carcinoma: A Meta-analysis. Am. J. Gastroenterol 109, 325–334. [PubMed: 24445574]
67. Browning JD, Kumar KS, Saboorian MH, and Thiele DL (2004). Ethnic differences in the prevalence of cryptogenic cirrhosis. Am. J. Gastroenterol 99, 292–298. [PubMed: 15046220]
68. Romeo S, Kozlitina J, Xing C, Pertsemlidis A, Cox D, Pennacchio LA, Boerwinkle E, Cohen JC, and Hobbs HH (2008). Genetic variation in PNPLA3 confers susceptibility to nonalcoholic fatty liver disease. Nat. Genet 40, 1461–1465. [PubMed: 18820647]
69. Aurnhammer C, Haase M, Muether N, Hausl M, Rauschhuber C, Huber I, Nitschko H, Busch U, Sing A, Ehrhardt A, and Baiker A (2012). Universal real-time PCR for the detection and quantification of adeno-associated virus serotype 2-derived inverted terminal repeat sequences. Hum. Gene Ther. Methods 23, 18–28. [PubMed: 22428977]
70. Guo P, El-Gohary Y, Prasadan K, Shiota C, Xiao X, Wiersch J, Paredes J, Tulachan S, and Gittes GK (2012). Rapid and simplified purification of recombinant adeno-associated virus. J. Virol. Methods 183, 139–146. [PubMed: 22561982]
71. Zhang Z, Funcke JB, Zi Z, Zhao S, Straub LG, Zhu Y, Zhu Q, Crewe C, An YA, Chen S, et al. (2021). Adipocyte iron levels impinge on a fat-gut crosstalk to regulate intestinal lipid absorption and mediate protection from obesity. Cell Metab 33, 1624–1639.e9. [PubMed: 34174197]
72. Wang S, Zhu Q, Liang G, Franks T, Boucher M, Bence KK, Lu M, Castorena CM, Zhao S, Elmquist JK, et al. (2021). Cannabinoid receptor 1 signaling in hepatocytes and stellate cells does not contribute to NAFLD. J. Clin. Invest 131, e152242. [PubMed: 34499619]
73. McDonald JG, Smith DD, Stiles AR, and Russell DW (2012). A comprehensive method for extraction and quantitative analysis of sterols and secosteroids from human plasma. J. Lipid Res 53, 1399–1409. [PubMed: 22517925]
74. Chalvardjian A, and Rudnicki E (1970). Determination of lipid phosphorus in the nanomolar range. Anal. Biochem 36, 225–226. [PubMed: 5482631]
75. Rexach MF, and Schekman RW (1991). Distinct biochemical requirements for the budding, targeting, and fusion of ER-derived transport vesicles. J. Cell Biol 114, 219–229. [PubMed: 1649197]
76. Rowe T, Aridor M, McCaffery JM, Plutner H, Nuoffer C, and Balch WE (1996). COPII vesicles derived from mammalian endoplasmic reticulum microsomes recruit COPI. J. Cell Biol 135, 895–911. [PubMed: 8922375]
77. Nohturfft A, Yabe D, Goldstein JL, Brown MS, and Espenshade PJ (2000). Regulated step in cholesterol feedback localized to budding of SCAP from ER membranes. Cell 102, 315–323. [PubMed: 10975522]

Highlights

- Inhibition of DGAT2 in hepatocytes shunts DAGs to phospholipid synthesis
- Inhibition of DGAT2 in hepatocytes increased PE concentrations in the ER
- Increased PE concentrations in the ER block SREBP-1 cleavage, reducing lipogenesis

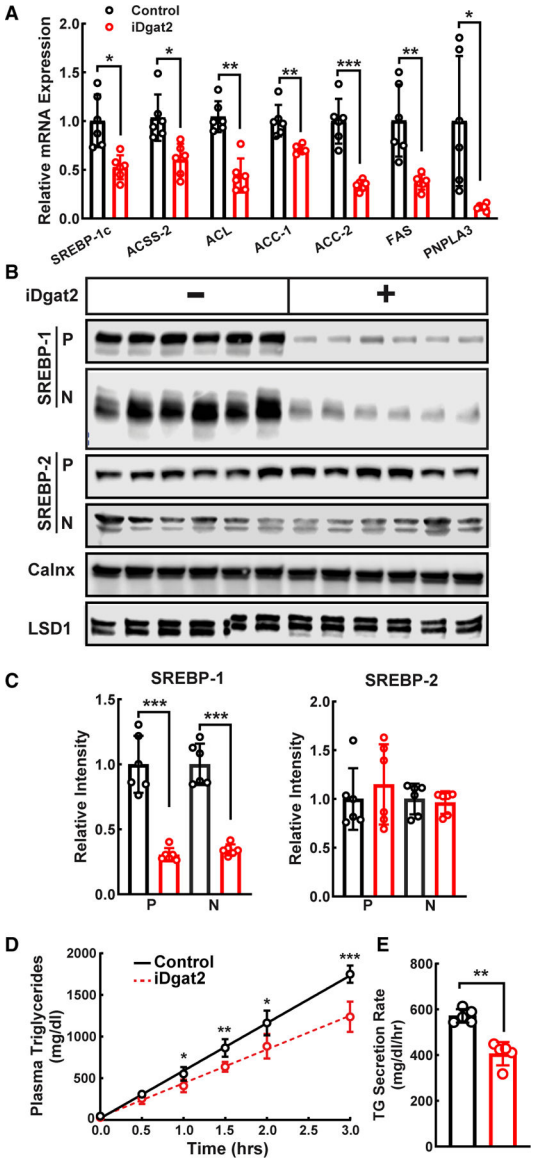

Figure 1. DGAT2 inhibition suppresses nSREBP-1 and reduces SREBP-1-regulated lipid synthesis and secretion

(A) Relative mRNA levels of genes involved in lipogenesis in livers of C57BL/6J mice that were fed chow or chow diet supplemented with iDgat2 (n = 6 per group). Total RNA was extracted from livers of control and iDgat2-treated C57BL/6J mice described in Table 1 and subjected to quantitative real-time PCR analysis. Expressions of the genes were normalized to cyclophilin.

(B) Immunoblot analysis of SREBP protein levels in C57BL/6J mice that were fed chow or chow diet supplemented with iDgat2. Membrane and nuclear proteins were prepared from individual livers, and immunoblot analysis was performed as described in the STAR Methods. Precursor SREBPs (P) were evaluated using membrane protein and activated nuclear forms of SREBPs (N) were measured using nuclear protein. Calnexin and LSD1 were used as loading controls for membrane and nuclear proteins, respectively.

(C) Protein intensities of immunoblots from (B) were quantified, and the intensities of precursor (P) and nuclear (N) SREBPs were normalized to calnexin and LSD1, respectively.
(D) Liver lipid secretion in C57BL/6J mice that were fed chow or chow diet supplemented with iDgat2 (n = 5 per group, 9 weeks of age). Male C57BL/6J mice were fed chow or chow diet supplemented with iDgat2 (0.004%) for 7 days. Mice were fasted for 4 h prior to the study.
(E) Plasma TG secretion rates were calculated for each mouse from the linear regression analysis of the time vs. TG concentrations. Data are the mean ± SD. Statistical significance was assessed by two-tailed Student's t test, *$p < 0.05$, **$p < 0.01$, ***$p < 0.001$.

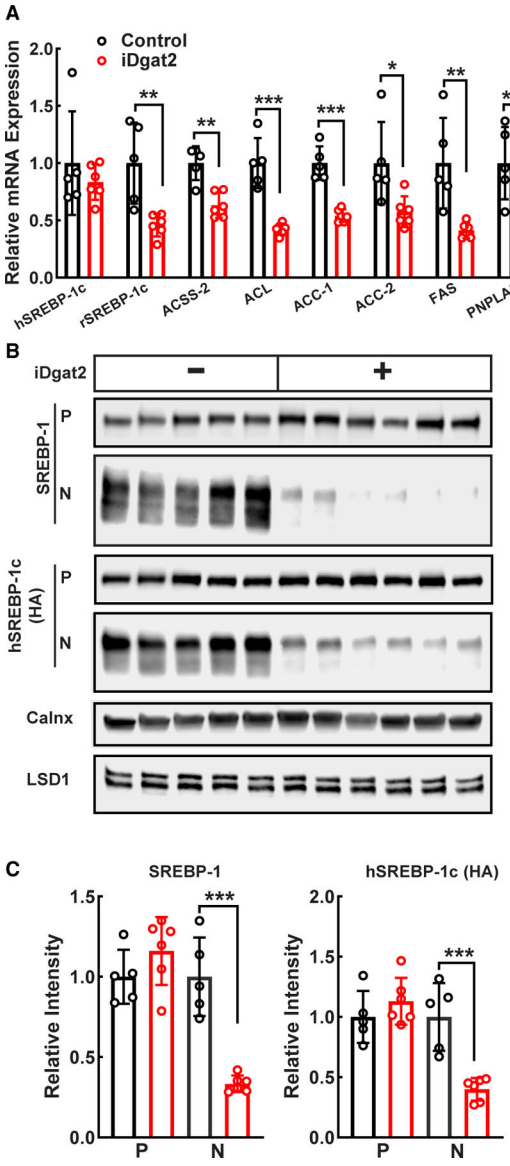

Figure 2. DGAT2 inhibition suppresses hepatic nSREBP-1 in TghSREBP-1c rats

(A) Relative mRNA levels of genes involved in lipogenesis in livers from TghSREBP-1c rats that were fed chow or chow diet supplemented with iDgat2 (n = 5–6 per group). Total RNA was extracted from livers of control and iDgat2-treated TghSREBP-1c rats described in Table 1 and subjected to quantitative real-time PCR analysis. Expressions of the genes were normalized to cyclophilin.

(B) Immunoblot analysis of SREBP-1 protein in TghSREBP-1c rats that were fed chow or chow diet supplemented with iDgat2. Membrane and nuclear proteins were prepared and subjected to immunoblot analysis as described in the STAR Methods. Precursor SREBPs (P) were measured in membrane protein and activated nuclear forms of SREBPs (N) were measured in the nuclear fractions. SREBP-1 denotes the total SREBP-1 (rat endogenous and human transgene). HA denotes the HA-tagged transgenic human SREBP-1 protein. Calnexin and LSD1 were used as loading controls for membrane and nuclear proteins, respectively.

(C) Protein intensities of immunoblots from (B) were quantified, and the intensities of precursor (P) and nuclear (N) SREBPs were normalized to calnexin and LSD1, respectively. Data are presented as mean ± SD. Statistical significance was assessed by two-tailed Student's t test, *p < 0.05, **p < 0.01, ***p < 0.001.

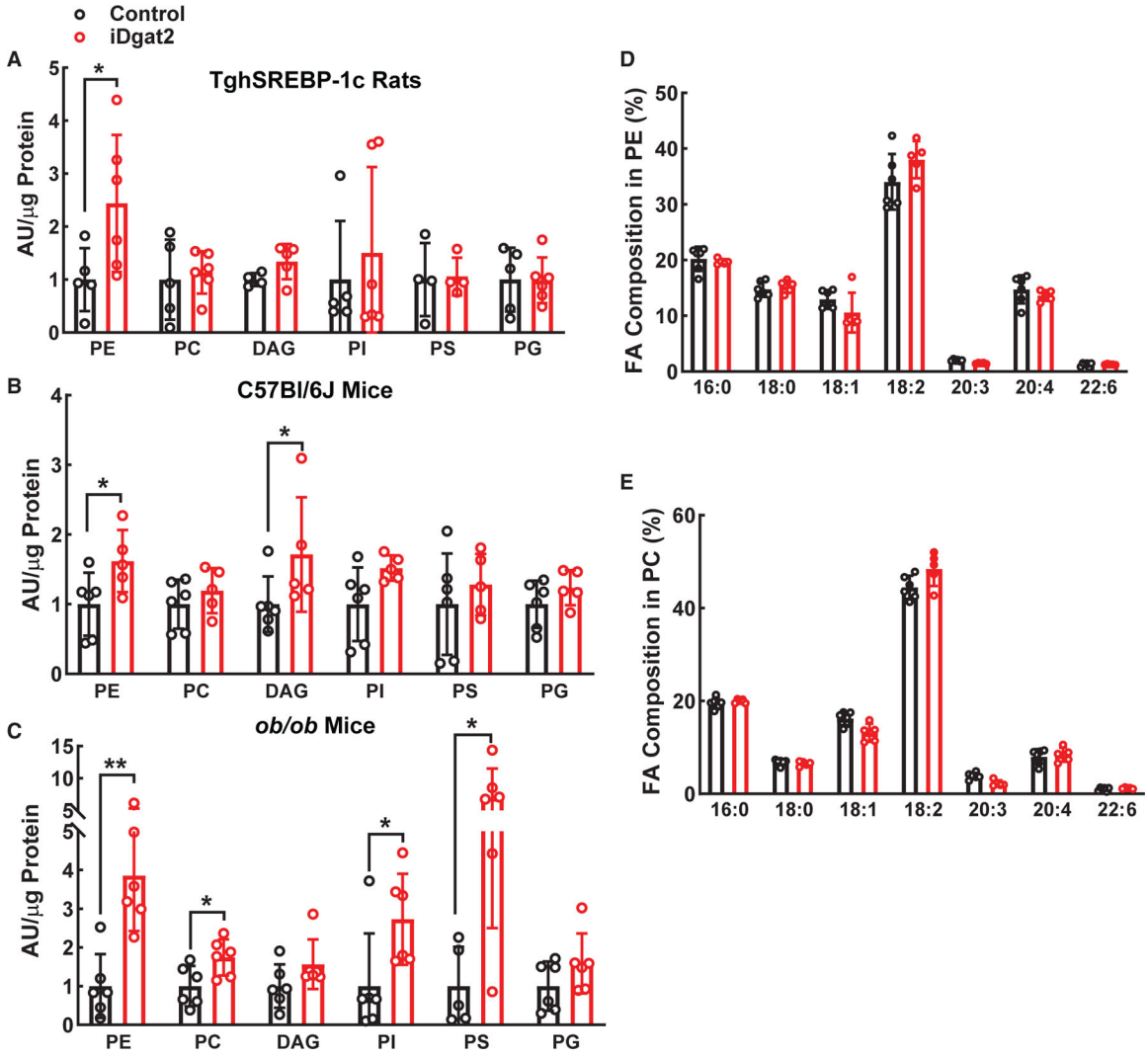

Figure 3. Lipidomic analysis of liver ER fractions from animals treated with iDgat2

(A–C) Lipid species of ER fractions prepared from iDgat2-treated TghSREBP-1c rats (n = 5 for control and n = 6 for iDgat2), C57BL/6J mice (n = 6 for control and n = 5 for iDgat2), and *ob/ob* mice (n = 6 per group). Lipids in the liver ER fractions of animals treated with iDgat2 were measured as described. Each individual value was normalized to the average value of the control group and shown as arbitrary units (a.u.)/μg protein.

(D and E) Fatty acid compositions of PC and PE in liver ER fractions of C57BL/6J mice. Data are presented as mean ± SD. Statistical significance was assessed by two-tailed Student's t test, *p < 0.05, **p < 0.01.

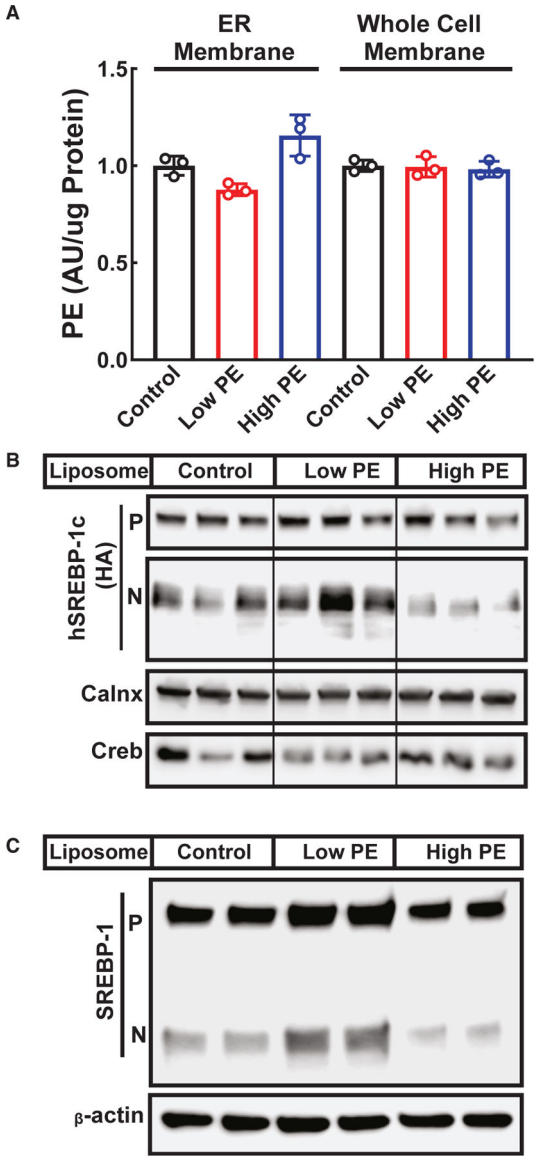

Figure 4. *In vitro* enrichment of PE in the ER suppresses SREBP-1 activation

Primary hepatocytes from TghSREBP-1c rats or Hepa-1c1c7 mouse hepatoma cells were treated with control, low-PE-containing liposomes, or high-PE-containing liposomes for 3 h as described in the STAR Methods.

(A) ER fractions and whole-cell membrane fractions were prepared from TghSREBP-1c rat primary hepatocytes, and PE levels in each fraction were measured.

(B) Immunoblot analysis of precursor and nuclear forms of hSREBP-1c in primary hepatocytes treated with liposomes containing different concentrations of PE. Membrane and nuclear proteins were prepared from the primary hepatocytes and subjected to immunoblot analysis.

(C) Immunoblot analysis of precursor and nuclear forms of SREBP-1 in Hepa-1c1c7 cells treated with liposomes containing different concentrations of PE. Whole-cell lysates were

prepared from the Hepa-1c1c7 cells, and SREBP-1 levels were evaluated by immunoblot analysis. P, SREBP-1 precursors; N, SREBP-1-activated nuclear form.

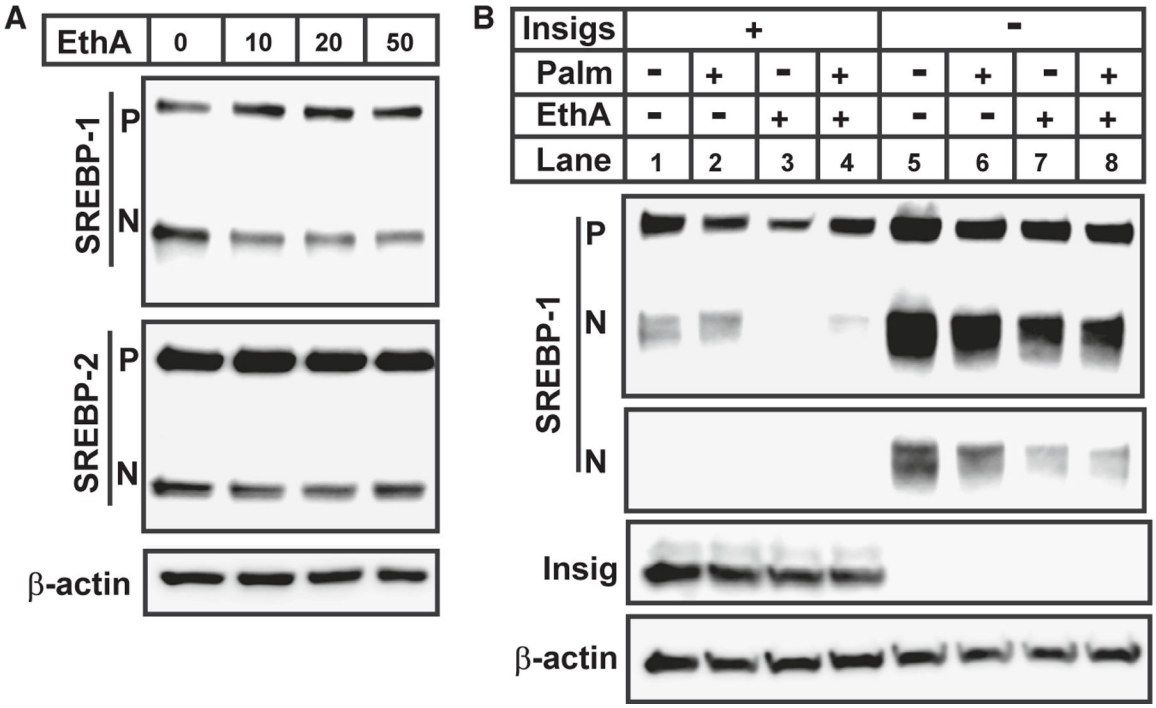

Figure 5. Insig is not required for the suppression of SREBP-1 cleavage by PE

Immunoblot analysis of precursor and nuclear forms of SREBP-1 in different cellular conditions.

(A) SV589 cells were cultured in DMEM with 5% lipoprotein-deficient serum supplemented with 0, 10, 20, or 50 μM ethanolamine (EthA) overnight. ALLN was added to the cells 2 h before the cells were harvested for immunoblot analysis.

(B) Control SV589 cells or SV589 cells that lack Insig-1 and Insig-2 were cultured in DMEM with 5% lipoprotein-deficient serum supplemented with vehicle (control, lanes 1 and 5), 100 μM palmitate (Palm, lanes 2 and 6), 100 μM EthA (lanes 3 and 7), or 100 μM of both Palm and EthA (lanes 4 and 8) overnight. ALLN was added to the cells 2 h before the cells were harvested. Protein was prepared from whole-cell lysates and applied to SDS-PAGE for immunoblot analysis. P, SREBP precursors; N, SREBP-activated nuclear forms. Nuclear forms of SREBP-1 in (B) high-exposure mode (upper) and low exposure mode (lower).

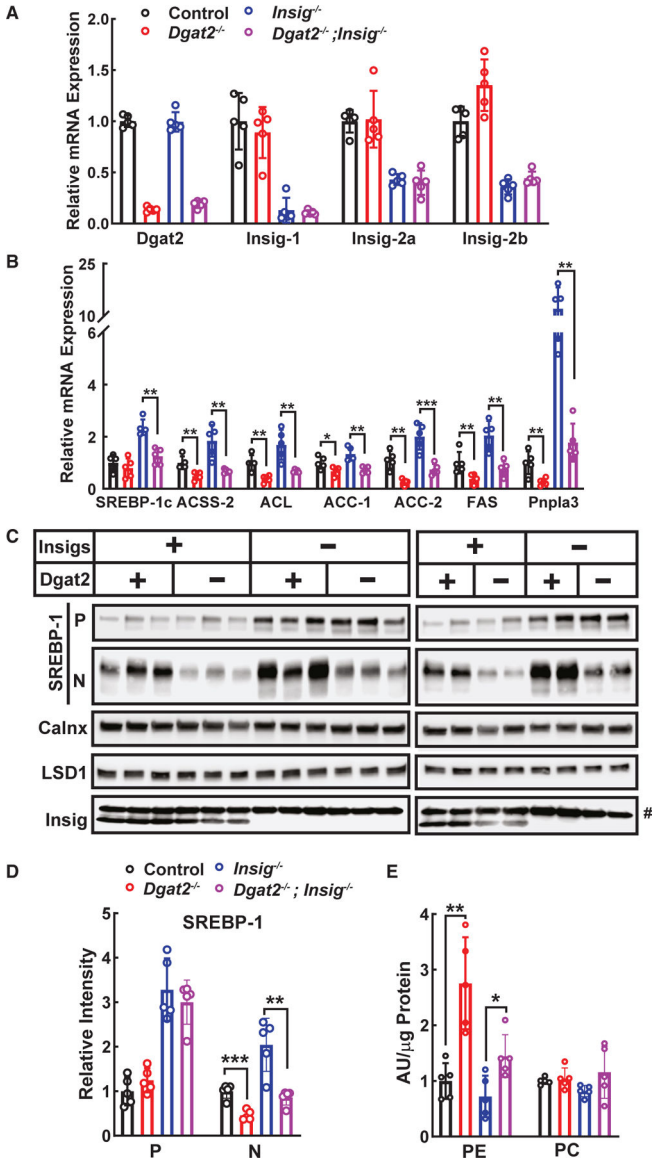

Figure 6. Liver ER PE concentrations in DGAT2-deficient mice in the presence or absence of Insigs

DGAT2 and/or Insigs were knocked out using sgRNAs packaged in AAV-DJ and injected into Cas9-expressing mice.

(A and B) Relative mRNA levels of Dgat2, Insig-1, Insig-2a, Insig-2b, and lipogenesis genes in Dgat2 and/or Insig-1 and −2 (Insig) hepatocyte-specific knockout mice (n = 5 per group). Total RNA was extracted from livers of the mice 6 weeks after the AAV injection and subjected to quantitative real-time PCR analysis.

(C) Immunoblot analysis of precursor and nuclear forms of SREBP-1 in Dgat2 and/or Insig knockout mice. Membrane and nuclear proteins from individual livers were prepared and loaded to 8% SDS-PAGE (3 samples from each group were loaded for the blot on the left panel, and the other 2 samples from each group were loaded for the blot on the right panel) and subjected to immunoblot analysis. Precursor SREBP-1 (P) and Insig proteins were detected in membrane fractions, and nSREBP-1 (N) was measured in the nuclear protein

fractions. Calnexin and LSD1 were used as loading controls for membrane and nuclear proteins, respectively.

(D) Protein intensities of immunoblots from (C) were quantified, and intensities of the precursor (P) and nuclear (N) SREBP-1 were normalized to calnexin and LSD1, respectively. # denotes a nonspecific bond detected by Insig antibody.

(E) PE and PC content in the ER fractions were measured using LC-MS/MS. Data are presented as mean ± SD. Statistical significance was assessed by two-tailed Student's t test. *$p < 0.05$, **$p < 0.01$, ***$p < 0.001$.

Table 1.

Phenotypic comparison of C57BL/6J mice and TghSREBP1c rats fed chow or chow supplemented with a DGAT2 inhibitor

	Mouse		TghSREBP-1c rat	
Parameters	**Control**	**iDgat2**	**Control**	**iDgat2**
Number of animals	6	6	5	6
Body weight (g)	27.5 ± 0.9	28.1 ± 0.9	369 ± 13	345 ± 22
Daily food intake (g)	4.1 ± 0.1	4.9 ± 0.5	21 ± 0.2	21 ± 0.7
Liver weight (% of body weight)	5.0 ± 0.1	4.8 ± 0.2	3.5 ± 0.0	3.5 ± 0.1
Liver TGs (mg/g liver)	9.38 ± 1.9	4.20 ± 0.3*	4.24 ± 0.3	2.84 ± 0.2**
Liver cholesterol (mg/g liver)	1.95 ± 0.0	1.94 ± 0.1	2.25 ± 0.1	2.46 ± 0.1
Plasma TGs (mg/dL)	129 ± 5.5	80.3 ± 6.1**	54.0 ± 4.5	21.8 ± 2.4**
Plasma cholesterol (mg/dL)	89.3 ± 6.9	53.7 ± 4.9**	84.8 ± 4.1	48.0 ± 1.8**
Blood glucose (mg/dL)	131 ± 9.4	151 ± 5.7	107 ± 4.9	103 ± 2.9
Plasma insulin (ng/mL)	0.51 ± 0.0	0.46 ± 0.1	1.20 ± 0.2	1.10 ± 0.4

Age-matched male C57Bl/6J mice and TghSREBP-1c rats were fed chow (control) or chow supplemented with iDgat2 (at a dose of 0.004% for mice and 0.01% for rats) for 7 days. Data were collected at the beginning of the light cycle and presented as mean ± SEM.

* and ** denote statistical significance of $p < 0.05$ and $p < 0.01$ (two-tailed Student's t test) between control and iDgat2-treated groups, respectively.

KEY RESOURCES TABLE

REAGENT or RESOURCE	SOURCE	IDENTIFIER
Antibodies		
Rabbit anti-SREBP-1	Rong et al.[33]	20B12
Rabbit anti-SREBP-2	Rong et al.[33]	22D5
Mouse anti-Insig	Jo et al.[55]	17H1
Rabbit anti-Calnexin	Enzo	Cat#ADI-SPA-860-F
Rabbit anti-β-actin	Cell Signaling	Cat#4970S
Rabbit anti-LSD1	Cell Signaling	Cat#2184
Rabbit anti-SCD-1	Cell signal	Cat#2794
Mouse anti-CREB	ThermoFisher	Cat#35-0900
Mouse anti-EEA1	Sigma-Aldrich	Cat#E7659
Mouse anti-Cytochrome C	Sigma-Aldrich	Cat#MAB1800
Mouse anti-NPC-2	Sigma-Aldrich	Cat#MABS440
Mouse anti-GM130	BD Biosciences	Cat#610822
Mouse anti-Prohibitin-1	Santa Cruz	Cat#sc-56467
Rabbit anti-LAMP1	Abcam	Cat#ab24170
Rabbit anti-α-tubulin	Abcam	Cat#ab6160
Mouse anti-PMP70	Sigma-Aldrich	Cat#SAB4200181
Mouse anti-His	Sigma-Aldrich	Cat#05-949
Rabbit anti-NaK ATPase	Abcam	Cat#ab76020
Rabbit anti-HA	Cell Signaling	Cat#3724
Rabbit anti-mCherry	Abcam	Cat#ab167453
Rabbit anti-ERGIC53 (LMAN-1)	Abcam	Cat#ab125006
Goat Anti-Rabbit IgG, $F(ab')_2$	Jackson Immuno	Cat#111-035-047
Goat Anti-Mouse IgG, $F(ab')_2$	Jackson Immuno	Cat#115-035-072
Li-COR IRDY 800 goat anti-Rabbit IgG	Fisher Scientific	Cat# NC9401842
Li-COR IRDY 680 goat anti-Mouse IgG	Fisher Scientific	Cat# NC0252290
Bacterial and virus strains		
pAAVscCB6	Gene Therapy Center at University of Massachusetts	Plasmid#P1023G10
AAV-DJ-eGFP	VectorBiolabs	Cat#7118
pAAV-CAG-shuttle-WPRE-GFP	Applied Viromics	Plasmid#0916
AAV-DJ Helper Free Expression System	Cell Biolabs	VPK-410-DJ
pAAV8	Addgene	Plasmid#112864
pX459 v2.0	Addgene	Plasmid#134451
Chemicals, peptides, and recombinant proteins		
DGAT2 inhibitor (PF-06424439)	Sigma-Aldrich	Cat# PZ0233
Tyloxapol (triton WR-1339)	Sigma-Aldrich	Cat#T8761

REAGENT or RESOURCE	SOURCE	IDENTIFIER
HPCD	ThermoFisher	Cat#NC0999732
His-tagged ALOD4	Infante and Radhakrishnan[40]	N/A
PC	Avanti	Cat#840052C
PE	Avanti	Cat#840021C
PI	Avanti	Cat#840042C
PS	Avanti	Cat#840032C
Ethanolamine	Sigma-Aldrich	Cat#398136
Palmitic acid	Sigma-Aldrich	Cat#P5585
Liberase	Sigma-Aldrich	Cat#5401127001
Dnase1	Sigma-Aldrich	Cat# 10104159001
HBSS, − Ca^{2+}, − Mg^{2+}, no phenol red	ThermoFisher	Cat#14175095
HBSS, + Ca^{2+}, + Mg^{2+}, no phenol red	ThermoFisher	Cat#14025092
Percoll	Sigma-Aldrich	Cat# P1644
OptiPrep™ Density gradient medium stock	Sigma-Aldrich	Cat# D1556
Flavopiridol	Sigma-Aldrichh	Cat# F3055
eBioscience™ 1× RBC lysis buffer	ThermoFisher	Cat#00-4333-57
ATP	Sigma-Aldrich	Cat#10519987001
GTP	Sigma-Aldrich	Cat#10106399001
Creatine kinase	Sigma-Aldrich	Cat#10127566001
Creatine phosphate	Sigma-Aldrich	Cat#10621714001
Fat free diet	MP biomedicals	Cat# 960238
Critical commercial assays		
RNA STAT-60 kit	TEL TEST	Cat#NC9489785
DNA-free, DNA removal kit	Invitrogen	Cat#1906
Taqman reverse transcription reagents	Applied Biosystems	Cat#N8080234
2× SYBR Green PCR master Mix	Applied Biosystems	Cat#4309155
Roche protease inhibitor	Rocke	Cat#1836170
SuperSignal West Pico Chemiluminescent Substrate	ThermoFisher	Cat#34580
10× Genomics Chromium Single Cell 3’ Library and Gel Beads Kit (version 3)	10× Genomics	Cat#1000075
Pierce BCA Protein Assay Kit	ThermoFisher	Cat#23225
Deposited data		
All single cell sequencing raw data	GEO repository	GSE250338
Uncropped high-resolution blots	Data S1-Source Data	N/A
Values used to create all graphs	Data S1-Source Data	N/A
Experimental models: Cell lines		
Hepa-1c1c7	ATCC	Cat#CRL-2026
SV589	Human Genetic Cell Repository	Cat#GM639
HEK293S GnTI	ATCC	Cat#CRL-3022

REAGENT or RESOURCE	SOURCE	IDENTIFIER
Experimental models: Organisms/strains		
C57Bl/6J mouse	Jackson Laboratory	Stock#000664
ob/ob mouse	Jackson Laboratory	Stock#000632
Cas9 knockin mouse	Jackson Laboratory	Stock#026179
TghSREBP-1c rat	Owen et al.[36]	N/A
Oligonucleotides		
5'-caccGCCAGAAGTGGTCGTGCAATC-3'	N/A	OL1243
5'-aaacGATTGCACGACCACTTCTGGC-3'	N/A	OL1244
5'-caccGAGCCTCGTGCTCTTCTCGGT-3'	N/A	OL1247
5'-aaacACCGAGAAGAGCACGAGGCTC-3'	N/A	OL1248
5'-caccGTCACCTGGGCCCAAAAAGTG-3'	N/A	OL1515
5'-aaacCACTTTTTGGGCCCAGGTGAC-3'	N/A	OL1516
5'-caccGATGCTTGCAATCACATCAGG-3'	N/A	OL1517
5'-aaacCCTGATGTGATTGCAAGCATC-3'	N/A	OL1518
5'-accGGATCTGCCCTGTCACGCGAG-3'	N/A	Dgat2sg-F
5'-aacCTCGCGTGACAGGGCAGATCC-3'	N/A	Dgat2sg-R
5'-accGCTGAGGATACGGCACTGGCG-3'	N/A	Insig-1sg-F
5'-aacCGCCAGTGCCGTATCCTCAGC-3'	N/A	Insig-1sg-R
5'-accGTGTGAACGTGGTGATCCGCG-3'	N/A	Insig-2sg-F
5'-aacCGCGGATCACCACGTTCACAC-3'	N/A	Insig-2sg-R
5'-accAACCCCTGATTGTATCCGCA-3'	N/A	Scramble-F
5'-aacTGCGGATACAATCAGGGGTT-3'	N/A	Scramble-R
Primers for quantitative real-time PCR see Table S1	N/A	N/A
Software and algorithms		
Image Studio™ Version 5.0	Li-COR	N/A